Molecular genetic studies on *Transmembrane Nine 1* for rhamnogalacturonan II deposition in *Arabidopsis thaliana*

ラムノガラクツロナン II 合成における

シロイヌナズナ *Transmembrane Nine 1* の分子遺伝学的研究

Akihiko Hiroguchi

廣口　覚彦

Division of Biosphere Science,

Graduate School of Environmental Science,

Hokkaido University

2021

Contents

学 位 論 文 内 容 の 要 旨

博士（環境科学）　　氏 名　廣口　覚彦

学 位 論 文 題 名

Molecular genetic studies on *Transmembrane Nine 1*
for rhamnogalacturonan II deposition in *Arabidopsis thaliana*
（ラムノガラクツロナン II 合成における
シロイヌナズナ *Transmembrane Nine 1* の分子遺伝学的研究）

【背景】

細胞接着は細胞同士もしくは細胞と細胞間隙をつなぎ合わせて組織を構築し、多細胞生物の個体発生および成長を支える。植物において、堅さと柔軟性の両方を持つ細胞壁が細胞接着の主要な役割をしている。細胞壁の最外層に位置する一次細胞壁の多糖はペクチン、セルロース、ヘミセルロースから構成されている。ペクチンはゲル状の性質をもち、セルロース繊維同士を接着する役割をしている。ペクチンにはホモガラクツロナン(HG)、ラムノガラクツロナン II (RG-II)、ラムノガラクツロナン I (RG-I)と呼ばれる多糖の構造領域があり、植物の必須微量元素であるホウ素は細胞内でホウ酸の形態で存在し、ホウ酸は RG-II を架橋する。ホウ酸による RG-II の架橋は正常なペクチンネットワークの形成に重要であり、ホウ素が不足した環境では架橋された RG-II が減少し、葉の展開や根の伸長の抑制、また不稔などの深刻な生育障害が生じる。RG-II は 12 種類以上の単糖から形成される複雑な構造を持つが、陸上植物の進化の過程で高度に保存されている。RG-II はゴルジ体で生合成され、小胞輸送により細胞外へ運ばれると考えられており、これら一連の過程を合成ととらえられる。これ

までに、RG-II 合成に関わる遺伝子が複数単離されているが、複雑な RG-II 合成の全体像はほとんど明らかになっていない。

既知の RG-II 合成変異株にはホウ素栄養応答が変化する株があることから、先行研究において RG-II 合成や RG-II 架橋に関わる因子を単離するため、ホウ素栄養応答に異常を持つシロイヌナズナ変異株が計 22 株単離された。本研究では類似した表現型を示した 2 株を対象とし、詳細な遺伝学的および生理学的解析によって RG-II 合成に関わる新たな分子の同定を目的とした。

【結果および考察】

ゴルジ体局在タンパク質の TMN1 の機能欠失によりホウ素栄養応答が変化した

固形培地の低ホウ素条件で野生型株は主根伸長が深刻に抑制されるのに対し、変異株の根は野生型株と比較して伸長した。ホウ素十分条件で変異株の根は野生型株と比較して伸長抑制を示した。この結果から、変異株のホウ素栄養応答に異常が生じていると考えられた。遺伝子マッピングと次世代シークエンサーのゲノム解析により、2 つの変異株が同一の遺伝子 *TMN1* に一塩基置換を持つことが分かった。一方の変異株 No.19 (*tmn1-1*)ではエキソン上に終止変異、もう一方の変異株 No.45 (*tmn1-2*)ではイントロンの 5'スプライスドナーサイトに変異が存在した。その結果、*tmn1-2* の cDNA には未成熟終止コドンが生じていた。さらに、*TMN1* に T-DNA 挿入をもつ *tmn1-3* も双方の変異株と同様の主根伸長の表現型を示したこと、*tmn1-1* での相補性試験から、TMN1 の機能欠失がホウ素栄養応答変化の原因であることが示された。加えて、顕微鏡観察により変異株の主根伸長変化は細胞伸長変化に起因することが観察され、TMN1 が根の細胞伸長に関わることが示された。TMN1 は 222 アミノ酸残基の N 末端領域に続き、9 回の膜貫通領域とさらに 18 残基の C 末端領域を持つ。TMN1 のアミノ酸配列は RG-II 合成に関わる既知のタンパク質と類似性を示さず、先行研究でゴルジ体に局在することが示されているが、分子の機能は不明であった。興味深いことに、*TMN1* の相同遺伝子はヒトを含む多くの真核生物で保存されているが、植物における変異株は報告されておらず、その生理学的機能は不明であった。

長期の水耕栽培における変異株のロゼット葉と根の乾燥重量が野生型株と比べて減少した

TMN1 変異株の個体成長を調べるため、蒸散および根の培地へのアクセスの点で固形培地よりも自然環境に近い水耕栽培栽培を行った。培地に低濃度、通常、高濃度のホウ素を加えた条件を設け、シロイヌナズナが栄養成長を続ける短日条件で成長を観察した。低ホウ素条件で変異株の根は野生型株より長く伸長し、固形培地と同様の表現型が再現された。一方で、いずれのホウ素条件でも変異株のロゼット葉のサイズと根の長さは減少し、乾燥重量も野生型株より減少した。つまり、低ホウ素条件の根の伸長の点では変異株のホウ素栄養応答が変化しているが、*TMN1* 変異株の個体成長はホウ素条件とは関係なく常に抑制されていた。

変異株の細胞壁中の RG-II と RG-I 量が野生型株と比較して減少した

TMN1 の生理学的機能を明らかにするため、ホウ素条件に関係なく引き起こされている変異株の個体成長抑制の原因を調べた。植物で示されているホウ素の作用点が細胞壁であるため、細胞壁中のホウ素濃度を測定した。ロゼット葉と根の細胞壁中のホウ素濃度は、極めて低濃度のホウ素条件において変異株と野生型株との間に減少は認められなかったが、マイルドな低ホウ素条件から高ホウ素条件において、変異株のホウ素濃度は野生型株よりも減少した。ホウ素が十分に存在する条件においては野生型株の RG-II の 90%以上がホウ酸に架橋されていると想定されるため、変異株ではホウ酸架橋された RG-II の量が減少していると考えられた。

上記の結果から、変異株では(1)ホウ酸による RG-II 架橋の効率が低下している可能性、(2)RG-II 自体の全体量が減少している可能性が考えられた。(1)の可能性を検証するためサイズ排除液体クロマトグラフィーにより、架橋された RG-II と架橋されていない RG-II を分離し、その屈折率のピーク面積から相対的な RG-II 架橋率を算出した。いずれのホウ素条件でも変異株の RG-II 架橋率が野生型株と比較して減少は認められなかったため、(1)の可能性は低いと考えられた。(2)の可能性を検証するため、RG-II 特異的に存在する 2-ケト-3-デオキシ糖を呈色反応により定量した。いずれのホウ素条件でも変異株のロゼット葉と根の 2-ケト-3-デオキシ糖は野生型株よりも 20%－30%減少したため、変異株の RG-II 自体の全体量が減少していると考えられた。さ

らに、RG-II 抗体を用いた免疫染色の結果、変異体でのシグナルの低下が示され、RG-II 量の減少が支持された。ホウ素条件に関係なくロゼット葉と根で見られた RG-II 全体量の減少は、変異株の乾燥重量の減少パターンと一致したため、RG-II 全体量の減少が変異株における乾燥重量の減少の一因であると考えられた。さらに産業技術総合研究所の協力によるロゼット葉の細胞壁中の単糖組成分析において、変異株のラムノース量の減少が観察された。細胞壁中のラムノースの多くは RG-I 由来であるため、変異株では RG-I 量も減少していると考えられた。これらより、TMN1 が細胞壁 RG-II や RG-I 量の維持に機能することが明らかにされた。

TMN1 の分子機能に関する知見を得るため、GFP タグを付加した TMN1 を *tmn1-1* 変異株に発現させ局在観察を行った。エキソサイトーシス阻害剤の BFA 処理下で、GFP-TMN1 の多くが脂質膜染色試薬 FM4-64 の BFA コンパートメントの周囲に観察された。この局在パターンは先行研究で示されているゴルジ体局在タンパク質と類似していた。さらに、細胞膜からのエンドサイトーシスを阻害する Dynasore 処理下で、GFP-TMN1 が細胞膜上に局在することは観察されなかった。このことから、大部分の GFP-TMN1 は細胞膜へ向かう輸送小胞には局在していないことが示された。よって TMN1 はペクチンを細胞外へ運ぶ働きよりも、ゴルジ体でペクチンを生合成する過程に機能していると考察された。

【結論】

本学位論文は、機能未知であった植物の TMN ファミリーがペクチン質多糖の RG-II と RG-I 合成において重要な因子であり、TMN1 が植物の正常な成長に必須であることを示した。また、*TMN1* 変異株の解析を通して、低ホウ素条件における細胞伸長がペクチン量によって制御されていることを明らかにした。本研究成果は植物の成長の分子機構に新たな知見を与えるものである。

List of abbreviations

aa	amino acid
AIR	alcohol-insoluble residue
BFA	brefeldin A
B	boron
bp	base pair
Ca	calcium
cDNA	complementary DNA
Col-0	Columbia-0
d	day(s)
dRG-II	dimeric RG-II
DAS	day after sowing
DNase	deoxyribonuclease
DW	dry weight
EMP	endomembrane protein
EMS	ethyl methanesulfonate
EPG	*endo*-polygalacturonase
FM4-64	N-(3-Triethylammoniumpropyl)-4-(6-(4-(Diethylamino)Phenyl) Hexatrienyl) pyridinium Dibromide
GFP	green fluorescent protein
h	hour(s)
HG	homogalacturonan
HPLC	high performance liquid chromatography
ICP-MS	inductively coupled plasma-mass spectrometry
min	minute(s)
mRNA	messenger ribonucleic acid
ORF	open reading frame

PCR	polymerase chain reaction
Phg1a	putative phagocytic receptor 1a
PI	propidium iodide
PR	primary root
RG-I	rhamnogalacturonan I
RG-II	rhamnogalacturonan II
rpm	revolution per minute
sec	second(s)
SP	signal peptide
TMN1	transmembrane nine 1
TM9SF	transmembrane 9 superfamily
T-DNA	transfer DNA
U	unit(s)
v	volume
WT	wild type

1. Introduction

Multicellular systems have enabled organisms to obtain diverse cellular functions for survival and adaptation to external environments. In multicellular organisms, tissue and organ formation is mediated by cellular adhesion. Adhesion receptors and cellular skeletons play a critical role for maintaining a large multicellular system for animals. In plants which are primary producers in ecosystems, the stiffness and plasticity of cell walls support cellular growth and organization. A primary cell wall is located at the outermost layer in cell wall, thus functioning in cell adhesion. It is mainly composed of cellulose, hemicellulose and pectin. Because pectin functions as a gel matrix where cellulose microfibrils are embedded, the pectic polysaccharide is an essential component of cell wall for cellular growth (Daher and Braybrook, 2015).

Pectin consists of galacturonic acid (GalA)-rich polysaccharides, including homogalacturonan (HG), rhamnogalacturonan-I (RG-I), and rhamnogalacturonan-II (RG-II) domains (Voragen *et al.*, 2009). HG is a major pectin component composed of a polymer of (α-1,4)-linked D-galacturonic acids. De-methylesterified HG chains are crosslinked through ionic bonding between calcium ion (Ca^{2+}) and carboxyl residues. This crosslinking of HG and Ca^{2+} is important for normal pectin network maintenance, which controls pectin gel properties. RG-I represents the second largest fraction of pectin; it contains a backbone consisting of repeating (α-1,2)-L-rhamnose-(α-1,4)-D-galacturonic acid and side chains. RG-II is a minor but highly conserved component in plants; it consists of a HG backbone linked to four distinct side chains composed of more than 12 different monosaccharides (O'Neill *et al.*, 2004). RG-II is crosslinked with borate between the two RG-II monomers, to form borate-dimerized RG-II through the formation of *cis*-diol ester bonds with apiosyl residues in side chain A. Boron (B) depletion has been reported to cause cellular adhesion and cell elongation disorders in plants through a reduction in the quantity of crosslinked RG-II (Ishii *et al.*, 2001; Iwai *et al.*, 2002; Chatterjee *et al.*, 2014; Camacho-Cristobal *et al.*, 2015).

Several proteins involved in pectin biosynthesis have been characterized. RG-II structure is synthesized in the Golgi apparatus by a variety of glycosyltransferases, using nucleotide diphosphate-linked sugars as activated donor substrates (Driouich *et al.*, 2012). Most nucleotide diphosphate-linked sugars are synthesized in the cytosol (Ahn *et al.*, 2006; Reboul *et al.*, 2011) and then transported into the Golgi (Sechet *et al.*, 2018). However, thus far, the overall molecular mechanism underlying RG-II polysaccharide synthesis in the Golgi and subsequent secretion to the apoplast remains poorly understood.

Recent studies have shown that the TRANSMEMBRANE NINE (TMN) protein family is involved in cellular attachment among eukaryotes including *Drosophila melanogaster*, *Dictyostelium discoideum*, *Saccharomyces cerevisiae*, and *Homo sapiens* (Cornillon *et al.*, 2000; Bergeret *et al.*, 2008; Froquet *et al.*, 2008; Paolillo *et al.*, 2015). TMNs belong to a superfamily of nine multi-spanning endomembrane proteins; they are highly evolutionarily conserved (Hegelund *et al.*, 2010). TMN proteins contain a long N-terminal domain with variable amino acid sequences, followed by nine transmembrane domains and a short tail on the C-terminus. TMN proteins in *Dictyostelium* and *Drosophila* interact with integrin-like protein and peptidoglycan recognition protein, respectively, for transport into the plasma membrane (Froquet *et al.*, 2012; Perrin *et al.*, 2015a, b). TMN proteins are localized to the Golgi apparatus in *Dictyostelium* and to intracellular vesicles or plasma membrane in *Drosophila*. TMN proteins may be involved in vesicular trafficking systems; they commonly contribute to cellular attachment among eukaryotes, despite their distinct interacting proteins and sub-cellular localization in different organisms. The presence of TMN is also conserved in plants; the Arabidopsis and *Oryza sativa* genomes have 12 and 17 paralogs, respectively. AtTMN1/EMP12 is localized to the Golgi apparatus (Gao *et al.*, 2012); however, its physiological function in plants has not yet been revealed.

In this study, a forward genetics approach was applied to identify a new component required for RG-II deposition or dimerization in cell walls, focusing on the

effects of altering B-dependent growth patterns, especially under low B conditions. This is because some RG-II synthesis mutants have shown impaired growth in response to changes in B concentrations caused by changes in the efficiency of borate-dimerized RG-II formation (O'Neill *et al.*, 2001; Voxeur *et al.*, 2011; Sechet *et al.*, 2018). Through characterization of the isolated mutants, the present thesis revealed that loss of function of *AtTMN1* partially relieved inhibition in root elongation under severely low B, and constantly reduced overall biomass compared with wild type plants, regardless of B conditions. It was suggested that the amounts of RG-II and RG-I were reduced in the cell wall of *tmn1* mutants, highlighting a role of Arabidopsis TMN1 in deposition of pectin in cell walls, for normal plant growth.

2. Materials and Methods

2.1. Plant materials and growth conditions

Arabidopsis thaliana (L.) Heynh. accession Columbia-0 (Col-0) was used as the wild type (WT). Plants were grown in solid or liquid media (Fujiwara *et al.*, 1992). Solid media contained 1% (w/v) sucrose and 1% (w/v) gellan gum (FUJIFILM Wako Pure Chemical, Japan). Boron (B) concentrations were adjusted with boric acid. For growth in solid media, surface-sterilized seeds were incubated in ultrapure water at 4 °C for stratification. Seeds were sown on solid media containing 0.1 μM (severely low B) or 100 μM (normal B) boric acid. They were incubated in a vertical position at 22 °C under a 16 h light/8 h dark cycle; light was provided by white fluorescent lamps (7 000–8 000 lux). To analyse vegetative growth, total B concentration in plant tissues and cell wall properties, Arabidopsis plants were germinated on rockwool with ultrapure water, and then incubated for 7 d. Seedlings were transferred into liquid media containing 0.1 μM (severely low B), 0.3 μM (mildly low B), 100 μM (normal B), and 500 μM (high B) boric acid; they were incubated for 38 d for vegetative growth and total B concentration analysis, and for 37 d for cell wall analysis. During the initial 14 d after the transfer, liquid medium was replaced weekly; subsequently, they were replaced at intervals of 3 d. Plants were grown at 70% relative humidity at 22 °C under short days (10 h light/14 h dark) to continue the vegetative growth stage. For reproductive growth tests, after plants had been incubated in water on rockwool for 7 d, they were grown for 68 d in liquid media supplemented with 0.1 μM, 0.3 μM, 100 μM, and 500 μM boric acid under long days (16 h light/8 h dark). Liquid medium was replaced weekly during the initial 14 d after transfer, and subsequently at intervals of 3 d or 4 d.

2.2. Mutant screening and genotyping of *tmn1-1*, *tmn1-2*, and *tmn1-3* mutants

For mutant screening, Col-0 seeds were mutagenized with ethyl methanesulfonate; 12 400 mutagenized M2 seeds were grown on solid media containing 0.03 μM boric acid, representing severe B deficiency and 114 plants showing longer roots were initially selected. Then, M3 seeds derived from self-pollination of the selected M2 plants, were grown on solid media under 0.03 μM and 100 μM B and mutant plants were screened for those showing longer roots compared with Col-0 under 0.03 μM (low B), but did not exhibit longer roots under 100 μM boric acid (i.e., sufficient B) supply. The mutant screening was performed in the previous study by Dr. K. Miwa and M. Tsukamoto.

Among 22 mutant candidates, two mutant lines, numbers 19 (*tmn1-1)* and 45 (*tmn1-2*), were investigated in this study. Isolated mutants 19 and 45 were crossed with Landsberg *erecta* (L*er*) and genetic mapping was conducted. The whole genome of each mutant was re-sequenced using the HiSeq2000 platform (Illumina, USA). The data were analysed using the DNA Data Bank of Japan Read Annotation Pipeline (Nagasaki *et al*., 2013) and the candidates responsible for mutations were found.

Single-nucleotide polymorphisms in *AtTMN1* were detected by dCAPS and CAPS markers for *tmn1-1* and *tmn1-2*, respectively. DNA fragments of the *AtTMN1* sequence were amplified by PCR using Primer 1 (P1) and P2 for *tmn1-1*, and P3 and P4 for *tmn1-2* (Table 5). The resulting fragments were then digested with *Taq*I for *tmn1-1* and *Mbo*I for *tmn1-2*.

tmn1-3 (WiscDsLoxHS217_03C), a T-DNA insertion line of *AtTMN1*, was originated from Col; the seeds were obtained from the Arabidopsis Biological Resource Center (USA). From the segregating population, plants homozygous for T-DNA were established by PCR using P5 and P6 for T-DNA insertions, and P6 and P7 for the WT genome (Table 5).

2.3. Detection of the full-length transcript of *AtTMN1*

Full-length transcripts of *AtTMN1* were detected by reverse transcription PCR. Plants were grown in solid media containing 100 μM boric acid for 11 d. Total RNA was extracted from leaves and roots using the RNeasy Plant Mini Kit (Qiagen, Germany). cDNA was synthesized using Prime Script RT Enzyme Mix (Takara, Japan). cDNA of *AtTMN1* and *ACTIN1* (cDNA quality control) were amplified using KOD-Plus-Neo (Toyobo, Japan) with specific primers P8 and P9 for *AtTMN1,* and P10 and P11 for *ACTIN1* (Table 5). cDNA from 5 ng (for *AtTMN1* and *ACTIN1* in rosette leaves), 10 ng (for *AtTMN1* in roots), and 1 ng (for *ACTIN1* in roots) of total RNA was used as template; 40 cycles of amplification were performed.

2.4. Measurement of cell lengths and cell numbers in roots

To obtain fully elongated cortical cell length measurements and meristematic cell counts, the root tips of plants grown on solid media were stained and observed. Under severely low B (0.1 μM), primary roots (PR) of 4-d-old plants were used, in which Col-0 had shorter roots than the *tmn1* mutants, but in which root tip cells had not severely collapsed. PRs were collected directly from solid media and stained with 10 μg ml^{-1} propidium iodide (PI; FUJIFILM Wako Pure Chemical, Japan) for 15 min, then rinsed twice in ultrapure water. Under normal B (100 μM), 11-d-old plants were used, in which root growth inhibition was obvious in the mutants. PRs were collected directly from solid media and stained with PI as described above for 40 min. Images were obtained using a confocal laser scanning microscope (LSM510, Zeiss, Germany). The excitation and detection wavelength windows were set at 488 and >540 nm, respectively. Up to three fully elongated cortical cells were selected from each PR; their longitudinal lengths were measured using ImageJ software (https://imagej.nih.gov/ij/). The numbers of cortical cells between the quiescent centre

and the first elongating cortical cell were counted in the PI-stained PRs. Counting was performed using the Cell Counter ImageJ plugin (https://imagej.nih.gov/ij/plugins/cell-counter.html).

2.5. Observation of columella cells in root tips

To examine root morphology, PR tips were stained as described above, with a slight modification to avoid root cap detachment during sampling. Plants were grown on solid media containing 100 μM boric acid for 14 d. PRs were cut; several drops of ultrapure water were placed on PRs while they remained on the media to ensure columella cells remained intact. Floating PRs were stained with PI for 5 min and observed by confocal laser scanning microscopy (LSM510, Zeiss, Germany).

2.6. Plasmid construction and plant transformation

In preparation for the complementation test and observation of the sub-cellular localization of GFP-AtTMN1 protein, new transgenic lines carrying *proAtTMN1:SP(AtTMN1)-GFP-AtTMN1genome* referring to a design described by Gao *et al.*, (2012) were generated. This construct was to express *GFP-AtTMN1* under the control of the endogenous *AtTMN1* promoter. Genomic nucleotides 3657117–3664330 of chromosome 1 sequences consisting of the putative promoter region (2.1 kb), ORF (4.3 kb), and terminator (0.7 kb), were amplified using Prime STAR HS DNA Polymerase (Takara, Japan) with primers P12 and P13 (Table 5). The fragments were cloned into the pENTR/D-TOPO vector using Gateway technology (Invitrogen, USA), and the plasmid was named pAH2. To construct *proAtTMN1:SP(AtTMN1)-GFP-AtTMN1genome*, three PCR fragments were assembled. The first fragment, which included a sequence encoding the AtTMN1 signal peptide (SP), was amplified from pAH2 using PCR, with primers P14 and P15 (Table 5). The second fragment, which

included *GFP*, was amplified using PCR, with primers P16 and P17 (Table 5). The third fragment, which included *AtTMN1* coding sequences, was amplified from pAH2 using PCR, with primers P18 and P19 (Table 5). The three fragments were mixed and then amplified using primers P14 and P19 (Table 5). The sequences encoding GGGGS between SP (26 aa) and GFP, and GGGSGGGS between GFP and AtTMN1 (27 aa) were inserted as linkers using the underlined primer sequences shown in Table 5. The resulting fragments were digested with *Sca*I and *Bam*HI; they were then ligated into the pAH2 vector, which had been treated with both enzymes. The resulting plasmid, *proAtTMN1:SP(AtTMN1)-GFP-AtTMN1genome* in pENTR/D-TOPO, was named pAH3. The insert in pAH3 was cloned into the destination vector pMDC99 (Curtis and Grossniklaus, 2003) by means of an LR reaction using Gateway technology (Invitrogen, USA), and the plasmid was named pAH6. pAH6 was introduced into *Agrobacterium tumefaciens* strain GV3101 (C58C1Rif^r) pMP90 (Gm^r), and *tmn1-1* plants were transformed using the floral dipping method (Clough and Bent, 1998). *proAtTMN1:SP(AtTMN1)-GFP-AtTMN1genome* was confirmed to be functional by testing the restoration of root growth inhibition of *tmn1-1* in the T_2 generation under 0.1 μM B. Among 30 independent transgenic lines, 20 exhibited full or partial complementation. For detailed analysis, a T_3 generation homozygous for T-DNA was established and four independent lines were used: pAH6-90-2, pAH6-100-1 (#1), pAH6-102-3, and pAH6-151-2 (#2).

2.7. Preparation of cell wall fractions from Arabidopsis rosette leaves and roots

For cell wall property analysis, alcohol-insoluble residues (AIRs) were prepared as previously described (Matsunaga and Ishii, 2006). Rosette leaves and roots were harvested from 44-d-old plants and then frozen. For each analysis, the following number of plants were collected as a single sample: B concentration, six for rosette leaves and four to nine for roots; ratio of dRG-II-B to total RG-II, six each for rosette

leaves and roots; 2-keto-3-deoxy monosaccharide concentration, three to six for rosette leaves and six to 12 for roots; monosaccharide composition, six for rosette leaves. The frozen materials were homogenized in 80% (v/v) ethanol. After the homogenates had been centrifuged, all insoluble pellets were washed with 80% (v/v) ethanol twice, 99.5% (v/v) ethanol once, chloroform/methanol (1:1, v/v) twice, acetone once, and ultrapure water twice. The AIRs were freeze-dried with FDU-1200 (EYELA, Japan) and treated as cell wall fractions. For monosaccharide composition analysis, rosette leaves were homogenized in 80% (v/v) ethanol. After the homogenates had been centrifuged, insoluble debris were washed with 80% (v/v) ethanol twice, 80% (v/v) ethanol overnight, 99.5% (v/v) ethanol once, chloroform/methanol (1:1, v/v) three times, acetone twice, and ultrapure water twice. The AIRs were freeze-dried as described above.

2.8. B and Ca concentration measurements

To measure total B concentrations, rosette leaves and roots of 45-d-old plants were harvested and rinsed with ultrapure water. The harvested rosette leaves and roots were dried at 60 °C for longer than 2 d and the dry weights were measured. After the samples had been dried, they were submerged in concentrated HNO_3 (60–61%) at 22–24 °C for 2 d, digested at 110 °C, then completely digested with H_2O_2 (30–35.5%) at 80 °C. The digested samples were dissolved in 2% HNO_3. B concentrations were measured by inductively coupled plasma-mass spectrometry (ICP-MS) (ELAN 6100 DRC-e, PerkinElmer, USA). To measure B and Ca concentrations in cell walls in rosette leaves and roots, 0.7–2.3 mg of AIR samples were submerged in concentrated HNO_3 at 22–24 °C for 2–4 d. The samples were digested as described above and then dissolved in 2% HNO_3. B and Ca concentrations were then determined by ICP-MS.

2.9. Determination of RG-II-B dimer formation in cell walls

To determine the ratio of dRG-II-B (RG-II-B dimer) to total RG-II in rosette leaf and root cell walls, the RG-II dimers and monomers were analysed as previously described (Matsunaga and Ishii, 2006) with slight modifications; 2.0–2.2 mg and 1.0–2.1 mg of AIRs were used for rosette leaves and roots, respectively. AIRs were saponified with 300 µl of 0.1 M NaOH at 4 °C for 4 h to remove methyl and acetyl esters; the supernatant pH was then adjusted to 5.0 with 10% (v/v) acetic acid. The suspensions were treated with six units (U) of *endo*-polygalacturonase (EPG) M1 for 24 h at 4 °C to release RG-II from AIRs. Before use, EPG from *Aspergillus niger* (Megazyme, Ireland) was dialysed with 0.1 M sodium acetate buffer. After the suspensions had been centrifuged, the supernatants were filtered through 0.45 µm membranes and subjected to size-exclusion HPLC/refractive index detection (HITACHI High Technologies Corporation, Japan) using a Diol-120 column (8 mm × 300 mm, YMC Co., Kyoto, Japan). The analyses were performed as follows: eluent, 0.2 M ammonium formate (pH 6.5); flow rate, 1.0 ml min^{-1}; and injection volume, 10 µl or 100 µl for rosette leaves and 100 µl, 150 µl, or 200 µl for roots. Relative proportions of dRG-II-B to total RG-II were calculated from the peak area of dRG-II-B and RG-II monomer.

2.10. Determination of 2-keto-3-deoxy sugars in cell walls

To estimate the quantities of RG-II in rosette leaf and root cell walls, 2-keto-3-deoxy (RG-II specific) sugars were measured using a modified thiobarbituric acid method (York *et al.*, 1985). Approximately 2.0 mg and 1.5 mg of AIRs were used for rosette leaves and roots, respectively. AIRs were saponified with 190.5 µl of 0.1 M NaOH at 4 °C for 8 h; the supernatant pH was adjusted to 5.5 with 10% (v/v) acetic acid. Cell walls were treated with 5 U of EPG M2 from *Aspergillus aculeatus* (Megazyme, Ireland) for 89 h at 35 °C for complete digestion. Before use, the enzyme was dialysed

with 0.1 M sodium acetate buffer. The suspensions were centrifuged and the supernatants were collected. This process was repeated three times to completely remove insoluble residues. The supernatant (200 µl) was mixed with 100 µl of 0.5 M H_2SO_4, then incubated for 30 min at 100 °C to hydrolyse polysaccharides into monosaccharides. The solutions were cooled for 10 min at 22–24 °C. Following this, 250 µl of 40 mM HIO_4 dissolved in 62.5 mM H_2SO_4, was added to the solution, which was then incubated for 20 min at 22–24 °C to generate formylpyruvic acid from oxidized 2-keto-3-deoxy sugars. Subsequently, 500 µl of 2% Na_2SO_3 dissolved in 0.5 M HCl, was added to the solutions to neutralize excess HIO_4. Then 500 µl of 25 mM thiobarbituric acid was added to the solutions, which were then incubated for 15 min at 100 °C to generate pigments. DMSO (99.5%, 1 ml) was added to the solutions, which were then incubated for 6–7 min at 22–24 °C to stabilize the pigments. The 548 nm absorbance of the pigments was measured using a spectrophotometer (U-3900/3900H, HITACHI High Technologies Corp., Japan). The quantities of 2-keto-3-deoxy sugars were calculated using 2-keto-3-deoxyoctonate ammonium salt (Sigma-Aldrich, USA) as a standard.

2.11. Observation of pectin distribution in cross-sections of roots

To observe pectin distribution, the PRs were embedded in LR White resin (Nisshin EM Corp., Japan); pectin was visualized with an indirect immunofluorescence method. Plants were grown on solid media containing 0.1 µM and 100 µM boric acid for 5 d. The PR tips were cut and then immersed with 4% paraformaldehyde dissolved in 20 mM sodium cacodylate buffer (pH 7.4) for 2 h at 4 ºC to fix cellular structures. The roots were immersed with 50% ethanol for 30 min at 4 ºC to be dehydrated. The process was performed with 60, 70, 80, and 90% ethanol for 30 min at each step, followed by 95% ethanol for 21 h at 4 ºC. Finally, the roots were immersed with absolute ethanol for 1 h at 4 ºC. Then the roots were infiltrated with 50% and 100%

LR White resin for 22.5 and 47 h, respectively, at 4 ºC. After transferring the roots into 100% LR White resin in 1.5 ml plastic tubes, the resins were incubated for 32 h at 60 ºC to polymerize completely. Serial root sections (0.99 µm) were prepared using an ultramicrotome (ULTRACUT N, Reichert-Nissei, Germany) and placed on coated glass slides (MAS-01, Matsunami Glass Industry, Japan). Section samples were treated with 2 N HCl for 15 min at 22–24 °C for epitope activation and then washed three times with phosphate-buffered saline (PBS: 137 mM NaCl, 2.7 mM KCl, 10 mM Na_2HPO_4, 2 mM KH_2PO_4, pH 7.4; FUJIFILM Wako Pure Chemical, Japan) for 42–6 (anti-RG-II antibody; Zhou *et al.*, 2018) or T/Ca/S buffer (20 mM Tris-HCl, pH 8.2, 0.5 mM $CaCl_2$, 150 mM NaCl) for 2F4 (anti-Ca^{2+} cross-linked HG antibody; PlantProbes, UK). For blocking, the sections were incubated with 10% normal goat serum (Thermo Fisher Scientific, USA) for 1 h at 22–24 °C and were then labelled with primary antibodies: 20 µg ml^{-1} anti-RG-II antibody, 42–6, and 1/10 anti-Ca^{2+} cross-linked HG antibody, 2F4 dissolved in 10% normal goat serum. They were incubated for 20 h at 4 ºC. After washing with the buffers three times, the sections were incubated with 20 µg ml^{-1} (1/100) goat anti-rabbit IgG (H+L) and 20 µg ml^{-1} (1/100) goat anti-mouse IgG1 antibodies conjugated to Alexa Fluor 488 (Thermo Fisher Scientific, USA) dissolved in 10% normal goat serum against 42–6 and 2F4, respectively, for 2 h at 22–24 °C. Following washing with the buffers three times, the sections were mounted with 50% (v/v) glycerol to be observed with a fluorescence microscope (DM2500, Leica, Germany). The Alexa Fluor 488 was excited with a mercury fluorescence source (EBQ 100-04-L, Leistungselektronik JENA GmbH, Germany) and observed through a 515 nm long-pass emission filter.

2.12. Cell wall monosaccharide composition analysis

To determine the monosaccharide composition of cell walls, extracted rosette leaf cell walls were analysed using an ultra-performance liquid chromatography–*p*-

aminobenzyl ethyl ester system (Sakamoto *et al.*, 2015) in coorperation with National Institute of Advanced Industrial Science and Technology. Approximately 2.00–3.00 mg of AIR were added to a 2 ml microtube, and starch contained in the AIR was digested with 1 ml of an amylase solution containing 500 U ml^{-1} of α-amylase from porcine pancreas (Megazyme, Ireland) and 0.33 U ml^{-1} of amyloglucosidase from *Aspergillus niger* (Megazyme, Ireland) in 0.1 M sodium malate buffer (pH 6.0) at 37 °C for 18 h. Insoluble residues in the amylase suspension were rinsed with absolute ethanol and ultrapure water, then dried completely at 60 °C overnight. The dried pellet was depolymerized with 50 µl of 72% (w/w) H_2SO_4 for 1 h with shaking at 1700 rpm. After the addition of 1.4 ml of ultrapure water to the AIR suspension, the AIR was hydrolysed at 121 °C for 1 h. The hydrolysed supernatant was neutralized with calcium carbonate powder and adjusted to around pH 5.0. Monomerized sugars in the neutralized supernatant were labelled with aminobenzyl ethyl ester solution containing 330 mg ml^{-1} of *p*-aminobenzyl ethyl ester (FUJIFILM Wako Pure Chemical, Japan), 66 mg ml^{-1} of sodium cyanoborohydride, 8% (v/v) acetic acid, and 75% (v/v) methanol at 80 °C for 30 min. Chromatographic separation and detection were conducted using an ACQUITY UPLC H-Class system equipped with an ACQUITY UPLC BEH C18 column (100 mm × 2.0 mm, 1.7 µm particle size, Waters Corp., USA) and fluorescence detector (ACQUITY UPLC FLR Detector, Waters Corp., USA) as previously described (Sakamoto *et al.*, 2015). For samples without amylase treatment, AIR powder was hydrolysed with H_2SO_4; monosaccharide composition in hydrolysate was analysed as described above. The monosaccharide composition analysis was done by Dr. S. Sakamoto (National Institute of Advanced Industrial Science and Technology).

2.13. Observation of GFP-AtTMN1 localization

To examine the molecular function of AtTMN1 protein, GFP-AtTMN1 localization was observed in the presence of exocytosis and endocytosis inhibitors using a confocal

laser scanning microscope (TCS SP5, Leica, Germany). Transgenic plants carrying *proAtTMN1:SP(AtTMN1)-GFP-AtTMN1genome* were grown for 5 d on solid media supplemented with 100 μM boric acid. In each treatment, chemicals were dissolved in liquid media containing 100 μM boric acid. Roots were incubated with 2 μM FM4-64 (Thermo Fisher Scientific, USA) for 5 min and then with 50 μM cycloheximide (Sigma-Aldrich, USA; a protein synthesis inhibitor) for 30 min. Subsequently, roots were treated with 50 μM brefeldin A (BFA; Sigma-Aldrich, USA; an exocytosis inhibitor) and cycloheximide for 60 min. The liquid media for BFA treatment contained 1.2% DMSO. To examine the possibility of AtTMN1 localization in the plasma membrane, 5-d-old transgenic plants grown under 100 μM B were treated with 100 μM Dynasore (Sigma-Aldrich, USA; an endocytosis inhibitor) for 90 min and then with 1 μM FM4-64 (Thermo Fisher Scientific, USA) for 30 s. The Dynasore liquid medium contained 1.7% DMSO. The laser excitation/detection wavelength bandwidths were 488/650–700 nm for FM4-64 and 488/500–530 nm for GFP.

To examine cell-type specific expression of AtTMN1 protein in roots, transgenic plants carrying *proAtTMN1:SP(AtTMN1)-GFP-AtTMN1genome* were grown for 5 d on solid media supplemented with 100 μM boric acid. PRs were collected directly from solid media and stained with 10 μg ml^{-1} PI for 1 min, then rinsed twice in ultrapure water. GFP and PI fluorescence in PRs was observed by the confocal laser scanning microscope. The laser excitation/detection wavelength bandwidths were 488/500–530 nm for GFP and 488/650–700 nm for PI. Their fluorescence was enhanced using Leica Application Suite Advanced Fluorescence Lite (2.6.0 build 7266; Leica, Germany).

2.14. Statistical analyses

Statistical analyses were performed using R software ver. 4.0.2. PR lengths were compared among plant lines using the Tukey–Kramer test. Comparison between Col-

0 and *tmn1* mutants in the other experiments were performed using Dunnett's multiple comparison test.

3. Results

3.1. *AtTMN1* mutations altered primary root growth in response to B nutrition

To isolate novel components of RG-II deposition or dimerization, Arabidopsis Col-0 seeds were mutagenized with ethyl methanesulfonate; 22 mutant candidates with an altered response to B were isolated, which showed longer roots only under low B in the previous study. Two independent mutants (nos.19 and 45) showed alleviation of root growth inhibition under low B, but exhibited reduced root growth under normal B conditions compared with WT Col-0 (Fig. 1A). The PR lengths of mutants nos.19 and 45 were 3.2-fold greater than the length of WT Col-0 under severely low (0.1 μM) B at 11 d after sowing (DAS; Fig. 1B). Under normal (100 μM) B, the PR lengths of mutants nos.19 and 45 were reduced by 13.4% and 20.4%, respectively, compared with Col-0; this indicated that B-dependent root growth was impaired in both mutants (Fig. 1B).

In the F_2 population derived from F_1 by crossing the mutants and WT L*er*, 19.7% and 14.8% of F_2 plants exhibited the mutant phenotype (i.e. alleviation of inhibition of root elongation under low B) in mutants nos.19 and 45, respectively (Table 1). Based on the segregation ratio, the phenotype appears to have been caused by a recessive mutation in a single genetic locus. Using a map-based cloning approach and genome analysis of the mutants, both mutants carried a single-base substitution (G to A) were found, but in a different position in *TRANSMEMBRANE NINE 1* (*AtTMN1/EMP12*; AT1G10950), which encodes a membrane protein of unknown function (Fig. 1C). AtTMN1 contains a long N-terminal domain followed by nine transmembrane domains, and is localized at the Golgi apparatus (Gao *et al.*, 2012). However, its mutant phenotypes have not been reported, and its physiological functions remain unknown.

Mutant no. 19 (*tmn1-1*) possesses a non-sense mutation in the 10th exon, which results in W355stop. Mutant no.45 (*tmn1-2*) carries a mutation in the 5’ splice donor site in the fifth intron (Fig. 1D). *tmn1-3*, a line carrying a T-DNA insertion in the

eighth intron of *AtTMN1*, showed similar growth to *tmn1-1* and *tmn1-2* under 0.1 μM B and 100 μM B (Fig. 1A, B), indicating that *AtTMN1* mutations were responsible for the phenotype.

To examine *AtTMN1* mRNA in the *tmn1* mutants, full-length transcripts of *AtTMN1* were investigated using reverse transcription PCR. In rosette leaves, *AtTMN1* cDNA was detected in *tmn1-1* and *tmn1-2*, but not in *tmn1-3* (Fig. 1E). The detected PCR product in *tmn1-1* corresponded with the size of the *AtTMN1* PCR product in Col-0, whereas the size of the major product in *tmn1-2* was slightly larger. Sequence analysis showed that the fifth intron (81 bp), where the mutation was present at the 5' splice donor site, was not spliced out; it remained within *tmn1-2* cDNA, resulting in a premature stop codon (Fig. 1D). Because proteins that are potentially translated from *tmn1-1* and *tmn1-2* mRNAs lack a large portion of the transmembrane domain at the C-terminus, functional AtTMN1 proteins are unlikely to be produced in *tmn1-1* and *tmn1-2* leaves. No transcript was detected in *tmn1* mutant roots (Fig. 1E), indicating that *AtTMN1* mRNA expression was below the detection limit in all three mutants, and that non-sense-mediated mRNA decay was induced in *tmn1-1* and *tmn1-2* in roots. Collectively, these results suggest that the *tmn1* mutants were loss-of-function mutants and that the mutant phenotypes were caused by loss of *AtTMN1* function.

To confirm that the loss of *AtTMN1* function was responsible for the mutant phenotypes, a complementation test was conducted by introducing a *proAtTMN1:SP(AtTMN1)-GFP-AtTMN1genome* construct into *tmn1-1* (no. 19), thereby expressing GFP-AtTMN1 fusion protein under the control of the native *AtTMN1* promoter. When T_3 homozygous lines (#1 and #2) were grown under 0.1 and 100 μM B conditions, abnormal root growth in *tmn1-1* (no. 19) was rescued, further supporting the notion that impaired B-dependent growth was caused by the loss of *AtTMN1* function (Fig. 1A, B).

According to an Arabidopsis Electronic Fluorescent Pictograph Browser (Winter *et al.*, 2007), *AtTMN1* mRNA was universally detected in roots, rosette leaves, internodes and siliques during vegetative and reproductive growths. To examine cell-

type expression of AtTMN1 in roots, GFP-AtTMN1 fluorescence was observed. GFP-AtTMN1 fluorescence was entirely detected in PR tips and weakly observed in the transition and mature zone where root hairs initiated. The fluorescence at the stele was relatively strong in any zone of the roots (Fig. 2). Furthermore, in PR tips, GFP-AtTMN1 was observed at the columella root cap; the intensity at a proximal end of root cap (Dolan *et al.*, 1993; Kumar and Iyer-Pascuzzi, 2020) tended to be higher compared with the other columella cells of distinct stages (Fig. 2). These results support that AtTMN1 is involved in root growth.

3.2. Root cell elongation was altered in *tmn1* mutants

To understand which process was altered in *tmn1* mutant root growth, the lengths of elongated cells in the root hair zone were measured and cells in the meristematic zone were counted at four DAS under 0.1 μM B and at 11 DAS under 100 μM B. Because incubation for longer than 4 d dramatically deformed root cell morphology under severely low B (0.1 μM), especially in Col-0, the root cells were observed at four DAS. Under 0.1 μM B, longitudinal lengths of fully elongated cortical cells were significantly increased by 31.2% and 27.3% in *tmn1-1* and *tmn1-2* (P<0.001; Fig. 3A, B), respectively, compared with Col-0. Conversely, under 100 μM B, cell lengths were significantly reduced by 11.0% and 10.6% in *tmn1-1* and *tmn1-2*, respectively (P<0.05; Fig. 3C, D). No significant differences in root meristem cell numbers were observed between Col-0 and the *tmn1* mutants under 0.1 μM or 100 μM B treatments (P>0.05; Fig. 3E–H). Our observations suggested that cell division was not primarily changed, but that cell elongation was affected in *tmn1* mutants under low and normal B conditions. Changes in cell length were positively correlated with changes in PR length in the *tmn1* mutants (Figs 1, 3); this suggested that the abnormal root growth observed in *tmn1* mutants was caused by changes in cell elongation.

The root tip morphology of seedlings grown in solid media under 100 μM B at 14 DAS showed that detaching root cap layers remained suspended from root tips in the *tmn1* mutants, but not in Col-0 (Fig. 4). This finding suggested a defect in the process of root cap maturation in *tmn1* mutants, in addition to altered cell elongation.

3.3. Leaf and root dry weights were reduced in *tmn1* mutants in hydroponic culture

To investigate long-term vegetative growth in the *tmn1* mutants, plants were grown hydroponically under short days. Rosette leaf sizes were markedly reduced in *tmn1* mutants, compared with Col-0, under all B treatments (Fig. 5A). Roots were longer in the *tmn1* mutants than in Col-0 under severely low B (0.1 μM), whereas the roots of *tmn1* mutants were shorter than the roots of Col-0 under 0.3 μM (mildly low), 100 μM (normal), and 500 μM (high) B conditions (Fig. 5B); these findings were consistent with mutant root phenotypes in solid media (Fig. 1A, B). Root bundles of the *tmn1* mutants appeared thinner than those of Col-0 under all B treatments (Fig. 5B). Thickness of individual root tips in *tmn1* mutants seemed to be reduced compared with Col-0 under 0.1 μM and 100 μM B (Fig. 6). Leaf and root dry weights were significantly reduced by 53.0–76.0% and 47.3–73.8% in the *tmn1* mutants under all B treatments including 0.1 μM B (P<0.01), when longer PRs were observed in the *tmn1* mutants than in Col-0 (Fig. 5C, D). This result indicated that overall biomass production in the vegetative stage was inhibited in the *tmn1* mutants, despite the presence of increased root elongation under severely low B treatment in the *tmn1* mutants.

To examine reproductive growth, plants were grown under long days. Although different growth responses to B deficiency by day length have been classically described (Warington, 1933), B-deficient symptoms in rosette leaf expansion and root elongation of Col-0 under low B did not appear to be largely affected by day length under our experimental regime. Similar to the vegetative growth results, the *tmn1* mutants displayed shorter roots under 0.3 μM (mildly low) B to 500 μM (high) B

treatments, but longer roots under 0.1 μM (severely low) B treatment, compared with Col-0 (Fig. 7C). Inhibited internode elongation and sterility were observed in Col-0 under severely low (0.1 μM) B and mildly low (0.3 μM) B treatments, whereas these disorders were partially recovered in the *tmn1* mutants, compared with Col-0 (Fig. 7A, B), which suggested that B-deficiency symptoms were relieved in the *tmn1* mutants. However, main stem length and branch numbers were reduced in the *tmn1* mutants, compared with Col-0, under 100 μM (normal) B and 500 μM (high) B treatments (Fig. 7A). Together, these results showed that AtTMN1 is necessary for normal growth in the vegetative and reproductive stages, irrespective of B conditions; moreover, *AtTMN1* mutations increase growth in specific tissues under low B conditions.

3.4. Cell wall B concentrations were lower in rosette leaves and roots of the *tmn1* mutants

To explore the mechanisms of impaired growth in the *tmn1* mutants, total B concentration per dry weight was determined in plants hydroponically grown under short days. In rosette leaves, no significant differences in total B concentration were observed between Col-0 and the *tmn1* mutants under 0.1 μM, 0.3 μM, or 100 μM B treatments (P>0.05; Fig. 8A). Under 500 μM B, leaf total B concentrations were significantly higher in *tmn1-1* compared with Col-0 (P<0.01), but not in *tmn1-2* or *tmn1-3* (P>0.05; Fig. 8A). Because no consistent changes in B concentrations were observed in mutant leaves, changes in total B concentration among leaves were presumably not a primary cause of the biomass reduction observed in Fig. 5C. In roots, total B concentration significantly decreased in *tmn1-3* under 0.1 μM B, *tmn1-2* under 0.3 μM B, and all three *tmn1* mutants under 100 μM B, compared with Col-0 (P<0.05; Fig. 8B). No significant differences were observed between Col-0 and the *tmn1* mutants under 500 μM B (P>0.05; Fig. 8B). Reduced B concentrations in roots under

normal B conditions may have caused the reduction in root growth observed in the *tmn1* mutants (Fig. 5D); however, reductions in root biomass observed under 500 μM B is not likely to be explained by changes in total B concentration in roots.

Because a primary physiological function of B in plants is pectic polysaccharide RG-II crosslinking in cell walls (O'Neill *et al.*, 2004), the AtTMN1 function in cell wall B concentration was next examined in plants hydroponically grown under short days. In rosette leaves, no significant differences in cell wall B concentration were observed between Col-0 and the *tmn1* mutants under 0.1 μM B (P>0.05; Fig. 9A). However, B concentrations were significantly (20.4–43.2%) lower in the *tmn1* mutants than in Col-0 in leaf cell walls under 0.3 μM, 100 μM, and 500 μM B treatments (P<0.01; Fig. 9A). In root cell walls, there were no significant differences between Col-0 and the *tmn1* mutants under 0.1 μM B (P>0.05; Fig. 9B). Under 0.3 μM B, B concentrations in root cell walls were significantly lower in *tmn1-1* (P<0.05); they also showed lower tendencies in *tmn1-2* and *tmn1-3* (Fig. 9B). Root cell wall B concentrations were significantly reduced by 24.9–36.3% in the *tmn1* mutants, compared with Col-0, under 100 μM and 500 μM B (P<0.01; Fig. 9B). Because B is predominately distributed to RG-II and nearly all RG-II is presumed to be crosslinked by borate in Col-0 under 100 μM B and 500 μM B treatments, the reduction of cell wall B concentration suggested that reduced quantities of borate-crosslinked RG-II were present in the *tmn1* mutants.

Calcium is another element in cell walls and it functions to cross-link de-methylesterified HG chains, a major domain of pectic polysaccharides. To verify the effects of AtTMN1 on Ca concentrations in cell walls, cell wall Ca concentrations were analysed. Rosette leaf cell wall Ca concentrations did not differ greatly between the *tmn1* mutants and Col-0 (Fig. 10A). Although significant increments were observed in *tmn1-1* under 0.1 μM, 0.3 μM, and 500 μM B and in *tmn1-2* under 500 μM B (P<0.05; Fig. 10A), these changes were not consistently observed in the leaf cell walls of *tmn1* mutants. In root cell walls, the *tmn1* mutants showed significant reductions in Ca concentration, compared with Col-0, under 0.1 μM and 0.3 μM B (P<0.05; Fig. 10B). Under 100 μM and 500 μM B, there were no significant differences between Col-0 and

the *tmn1* mutants (*P*>0.05; Fig. 10B). In immunostaining with 2F4 which recognizes Ca^{2+} cross-linked HG, the signal at the lamella of cortex periphery tended to be decreased in 5-d-old *tmn1-1* and *tmn1-2* grown on solid media under 0.1 μM B compared with Col-0, suggesting potential reduction of Ca^{2+} cross-linked HG in the mutants under low B (Fig. 10C).

Unlike the observed reduction in cell wall B concentrations, consistent patterns of changes in cell wall Ca concentrations were not found in the *tmn1* mutants, which suggested that the *AtTMN1* mutations predominately caused the observed reduction in cell wall B concentrations. Thus, reduced borate-cross-linked RG-II could be involved in the development of these impaired growth patterns.

3.5. Cell wall RG-II was reduced in *tmn1* mutant rosette leaves and roots

Two explanations were considered for the reduction of borate-dimerized RG-II based on lowered cell wall B concentrations in *tmn1* mutants (Fig. 9): (i) reduced efficiency of dimeric RG-II-B formation, and (ii) diminished total quantity of cell wall RG-II in the *tmn1* mutants. To test the first possibility, the relative proportion of dRG-II-B to the proportion of total RG-II was determined in cell walls of plants hydroponically grown under short days. In leaves, relative rates of RG-II cross-linking in cell walls were significantly higher in the *tmn1* mutants than in Col-0 under 0.1 μM B (*P*<0.05; Table 2). Under 0.3 μM, 100 μM, and 500 μM B, there were no significant differences in cross-linking rates between leaves of Col-0 and leaves of *tmn1* mutants (*P*>0.05; Table 2). In roots, cross-linking rates were significantly higher in *tmn1-3* under 0.1 μM B and in the three mutants under 0.3 μM B, compared with Col-0 (*P*<0.05; Table 2). Under 100 μM and 500 μM B, there were no significant differences between Col-0 and the *tmn1* mutants (*P*>0.05; Table 2). The lack of reduction in the relative proportions of dRG-II-B to total RG-II in the mutant cell wall likely refutes the hypothesis of lowered efficiency in dRG-II-B formation in the *tmn1* mutants.

To determine whether total quantities of RG-II were reduced in the *tmn1* mutants, 2-keto-3-deoxy sugars were measured in cell walls. In plants, 2-keto-3-deoxy sugars, (2-keto-3-deoxy-D-lyxo-heptulosaric acid and 3-deoxy-D-manno-oct-2-ulosonic acid) have been found only in RG-II; thus, their quantities represent the entire quantity of RG-II. The concentration of 2-keto-3-deoxy sugars in leaf cell walls were significantly reduced by 19.9–32.7% in the *tmn1* mutants, compared with Col-0, under all B treatments (P<0.001; Fig. 11A). Similarly, the concentration of 2-keto-3-deoxy sugars in root cell walls were significantly reduced by 25.5–32.8% in the *tmn1* mutants, compared with Col-0, under all B treatments (P<0.01; Fig. 11B). The reduced amount of 2-keto-3-deoxy sugars in cell walls indicates that total quantities of cell wall RG-II are diminished in both rosette leaves and roots of the *tmn1* mutants compared with Col-0, irrespective of B conditions.

To examine RG-II distribution, RG-II was visualized in cross-sections of PRs grown on solid media by labelling with an RG-II antibody. In meristematic zone of roots, signal intensities in the stele and the cortex periphery were decreased in the *tmn1* mutants compared with Col-0, whereas there were no apparent differences in the epidermis (Fig. 11C). In elongation zone of the roots, the signals in the cross-sections were entirely reduced in the *tmn1* mutants compared to Col-0 (Fig. 11D). This observation supports that RG-II amounts were reduced in both the meristematic and elongation zones of the roots in the *tmn1* mutants.

These results demonstrate that AtTMN1 is necessary for maintenance of the quantity of RG-II in cell walls. Because these reductions are consistent with the reductions of dry weight under all B conditions, it is highly likely that reduced quantities of RG-II, which cause a reduction in borate-dimerized RG-II, are at least partly responsible for the biomass reductions and altered growth responses observed in the *tmn1* mutants under severely low B conditions.

3.6. Quantities of cell wall RG-I were also reduced in the rosette leaves of *tmn1* mutants

To investigate whether cell wall components other than RG-II were affected by the lack of AtTMN1, the quantities of 10 monosaccharides were determined in leaf cell walls of plants grown with 100 μM B under short days. Regardless of the presence of amylase treatment, rhamnose content was significantly reduced by 21.2–27.3% in the *tmn1* mutants, compared with Col-0 (P<0.001; Table 3,4) The quantity of GalA (a substantial component of HG) was significantly reduced by 6.5% in *tmn1-1* cell walls treated with amylase, and by 14.8% and 17.3% in *tmn1-1* and *tmn1-2* cell walls without amylase treatment, respectively (P<0.05 ; Table 3,4). Glucose, xylose, mannose and glucuronic acid contents were significantly increased in the *tmn1* mutants, compared with Col-0, in cell walls treated with amylase (P<0.05; Table 3,4). Because rhamnose in cell walls is largely derived from RG-I, these reductions in rhamnose contents suggested that quantities of RG-I were also reduced in the cell walls of the *tmn1* mutants. Additionally, quantities of HG may have decreased slightly in the *tmn1* mutants. This observation suggests that AtTMN1 functions in the deposition of pectic polysaccharides in cell walls, especially RG-II and RG-I.

3.7. GFP-AtTMN1 BFA responses were largely similar to those of Golgi proteins

It has been reported that AtTMN1 is localized in the Golgi apparatus in Arabidopsis (Gao *et al*., 2012). RG-I and RG-II structures are synthesized at the Golgi apparatus by a variety of glycosyltransferases (Driouich *et al.*, 2012); packaged pectic polysaccharides are then delivered into the apoplast matrix via two *trans*-Golgi

network derived pathways (Sinclair *et al.*, 2018). Therefore, it was hypothesized that AtTMN1 functions in pectin biosynthesis in the Golgi apparatus and/or in secretion to the apoplast. To gain insight into the molecular function of AtTMN1, GFP-AtTMN1 localization was observed in the presence of exocytosis and endocytosis inhibitors. Under treatment with 50 μM BFA (an exocytosis inhibitor) accompanied by cycloheximide for 60 min, ring-like localization of GFP-AtTMN1 was mainly observed on the BFA compartment (Robinson *et al*., 2008) of FM4-64 (an endocytosis tracer; Fig. 12A). The distribution pattern of GFP-AtTMN1 was similar to the pattern of ST-mRFP (Naramoto *et al.*, 2014), confirming the localization of GFP-AtTMN1 mainly in the Golgi apparatus. Furthermore, under 90 min treatment with 100 μM Dynasore (a dynamin-dependent endocytosis inhibitor), GFP-AtTMN1 fluorescence signals did not show co-localization with FM4-64 on the plasma membrane (Fig. 12B). This suggested the likelihood that most of the GFP-AtTMN1 was neither localized to trafficking systems nor targeted to the plasma membrane. From these observations of GFP-AtTMN1 localization, it was inferred that AtTMN1 plays a role in pectin biosynthesis in the Golgi apparatus, rather than in trafficking pectin to the apoplast.

4. Discussion

4.1. AtTMN1 plays a role in pectic polysaccharide deposition in cell walls

In this study, AtTMN1 was identified as a novel component required for pectin deposition, which governs cell elongation and consequently overall plant growth. Arabidopsis mutants with impaired growth responses to low B nutrition were screened, based on prior observations that deficits in RG-II synthesis lead to altered responses to B nutrition (O'Neill *et al.*, 2001; Sechet *et al.*, 2018). In the *tmn1* mutants, quantities of RG-II, represented by 2-keto-3-deoxy sugar concentrations, and RG-I, represented by rhamnose contents, were decreased by 20–30% in leaf and root cell walls under all B treatments (Fig. 11; Table 3,4), which demonstrated that AtTMN1 was essential for normal pectin deposition in cell walls.

Considering the importance of RG-II and RG-I in cell growth (O'Neill *et al.*, 2001; Oomen *et al.*, 2002; Delmas *et al.*, 2008; Kobayashi *et al.*, 2011; Liu *et al.*, 2011), these results suggested that reductions of RG-II and RG-I contents were the main causes of cell elongation inhibition (Fig. 3C, D). Meanwhile, the *tmn1* mutants exhibited no apparent abnormalities of cell division (Fig. 3E-H) despite the reduced RG-II amounts in the meristematic zone of the PRs (Fig. 11C), implying that the RG-II reduction in the *tmn1* mutants was not so severe as to cause defects in cell division. This view is supported by the observation that reduced B-crosslinked RG-II under B deficiency primarily impairs cell elongation (Camacho-Cristóbal *et al.*, 2015). Thus, it is assumed that the cell elongation inhibition rather than the defect of cell division resulted in whole-plant growth and developmental impairment in the *tmn1* mutants. This is demonstrated by a reduction of dry weight in the vegetative growth stages under all tested B conditions, as well as impaired reproductive growth under sufficient B supply (100 µM and 500 µM; Fig. 5; Fig. 7). The assumption is supported by the prior observation that a 20% reduction in borate dimerized RG-II likely caused

dwarfism in Arabidopsis *mur1* and *GDP-D-mannose 3,5-epimerase*-silenced tomato plants with impaired RG-II structure (O'Neill *et al.*, 2001; Voxeur *et al.*, 2011).

4.2. Altered pectin affects growth under limited B conditions

Under severely low B, the *tmn1* mutants displayed alleviation of root elongation inhibition and reproductive growth failure compared with WT plants (which exhibited reduced growth) (Figs 1, 5, 7). In roots, this phenomenon was caused by increment of cell elongation in the *tmn1* mutants (Fig. 3A, B), in contrast to inhibition of cell elongation under B sufficiency (Fig. 3C, D). Cell elongation is generally inhibited under low B conditions, and pollen tube elongation is suppressed by B depletion, resulting in plant sterility (Dell and Huang, 1997; Huang *et al.*, 2000; Wang *et al.*, 2003). Therefore, it is concluded that the alleviation of cell elongation inhibition in the corresponding tissues explained the *tmn1* mutant phenotypes under severely low B conditions.

Cell enlargement in specific tissues of the *tmn1* mutants, compared with Col-0, may have been caused by reduction of overall pectin content, through cell wall loosening under severely limited B, when cell elongation was severely inhibited in Col-0. In roots, reduction of Ca^{2+} cross-linked HG (Fig. 10C) could cause cell wall loosening and result in increased cell elongation in the mutants under severely low B. However, based on the assumption that RG-II cross-linking by borate is a primary determinant for growth under low B, reduced RG-II content might be a major contributing factor in the increment of cell elongation in the *tmn1* mutants under limited B supply. In mutant cell walls under severely low B, B concentrations and total RG-II content were reduced, compared with WT plants (Figs 9, 11); this suggested that absolute quantities of dRG-II-B and monomeric RG-II had decreased. Considering that B deficiency inhibits cell elongation in WT through the reduction of dRG-II-B and increase in monomeric RG-II contents compared with plants under sufficient B supply, the reduction in monomeric RG-II, but not in dRG-II-B, in the *tmn1* mutants likely resulted in the alleviation of cell

elongation inhibition under severely low B conditions. This hypothesis is consistent with the findings in a previous study, where differences in tolerance to low B among rapeseed genotypes were reportedly defined by low quantities of pectin, presumably in the form of monomer RG-II (Zhou *et al.*, 2017). Our results further suggest that altered pectin, mainly RG-II, modifies plant growth under limited B supply.

Several homologs of the *Catharanthus roseus* receptor-like kinase subfamily have been shown to play regulatory roles in cell expansion by binding cell wall polysaccharides or glycosylated proteins (Nissen *et al.*, 2016). These proteins (e.g., FER, a receptor kinase that interacts with the pectin polysaccharide backbone) may sense the disruption of pectin cross-linking by B and Ca^{2+} (Feng *et al.*, 2018); these proteins may perceive monomeric RG-II and modulate cell elongation under limited B conditions.

4.3. The TMN protein family shares cell adhesion functions among eukaryotes

TMN proteins are conserved as the transmembrane 9 superfamily (TM9SF) among eukaryotes; some of these proteins have been characterized in organisms other than plants. Down-regulation of human TM9SF4, which belongs to the other cluster from AtTMN1 in the phylogenetic tree separated into two clusters (Hegelund *et al.*, 2010), has been shown to reduce adhesion of myelomonocytic cells to fibronectin (Paolillo *et al.*, 2015). In *Drosophila,* a null mutant of putative phagocytic receptor 1a (*Phg1a*; an ortholog of *TM9SF4*) showed defective phagocytosis against wasp eggs (Bergeret *et al.*, 2008). Given that haemolymph cells can recognize and attach to invaders, the *Drosophila phg1a* mutant may lose the capacity for cellular attachment under these conditions.

In *Dictyostelium*, a unicellular organism, the number of cells adhering to hydrophilic glass surfaces was reduced in a *Phg1A*-knockout mutant (Cornillon *et al.*, 2000). Similarly, the triple mutant *S. cerevisiae tmn1 tmn2 tmn3* displayed reduced

adhesion to solid yeast extract–peptone–dextrose medium surfaces and a concurrent filamentous growth defect (Froquet *et al.*, 2008), such that single yeast cells assembled into a multicellular form in response to nitrogen starvation (Mösch and Fink, 1997; Cullen and Sprague, 2012). Together, these data show that *TMN* family members are essential for intercellular attachment among eukaryotes, including both multicellular and unicellular organisms, although the regulation systems and molecules involved in cell attachment are distinct among organisms.

The *AtTMN1* mutations impaired the detachment of the proximal end of root cap, consistent with its expression (Figs 2, 4). The previous studies on loss-of-function mutants in pectin biosynthesis and degradation demonstrated that proper pectin metabolism is required for root cap maturation (Durand *et al.*, 2009; Bennett *et al.*, 2010; Kamiya *et al.*, 2016). Although the *tmn1* phenotype does not agree with a hypothesis that reduced amounts of pectin including HG promotes the root cap detachment, it is suggested that Arabidopsis TMN1 contributes to appropriate intercellular attachment of columella cells through proper pectin deposition. Considering that normal pectin is required for plant cell adhesion (Bouton *et al.*, 2002; Iwai *et al.*, 2002), it is believed that *AtTMN1* in plants also contributes to the biological processes involved in cellular attachment mediated by pectin deposition.

4.4. AtTMN1 might be involved in vesicular trafficking for pectin biosynthesis

The *TMN* families have been reported to control surface localization of cargo molecules at the plasma membrane. In *Dictyostelium*, surface levels of SibA (an integrin beta-like protein) were reduced in a *Phg1A*-knockout mutant defective in phagocytosis and cellular adhesion (Froquet *et al.*, 2012). Golgi-localized Phg1A interacted with glycine-rich residues in SibA transmembrane domains, which are necessary for its proper localization to the plasma membrane (Perrin *et al.*, 2015a). These findings indicate that the TMN homolog functions as a cargo receptor of integrin

molecules for cell–cell adhesion in this organism. In *Drosophila*, TM9SF4 (a TMN1 homolog) interacts with peptidoglycan recognition protein (a phagocytotic receptor) and has been shown to localize to intracellular vesicles and the plasma membrane. Thus, the *TM9SF4*-null mutant displays reduced peptidoglycan recognition protein transport into the cell surface, resulting in defects in phagocytosis in response to bacterial invasion (Perrin *et al.*, 2015b). Molecular analysis of TM9SF4 has suggested that *TMN* family members recognize these cargo molecules to secrete them into the cell surface in diverse organisms.

The molecular functions of a TM9SF4 human homolog have been well studied in metastatic melanoma cells that exhibit high expression of this protein. *TM9SF4* knockdown led to phagocytosis disorders and reduced activity of cannibal tumor cell (Lozupone *et al.*, 2009). In TM9SF4 knockout HEK293T cells of human, a reporter protein fused with six glycine residues of the SibA transmembrane domain was found to be stacked in the endoplasmic reticulum, whereas *TM9SF4* overexpression enhanced reporter localization to the plasma membrane (Perrin *et al.*, 2015a). These findings also suggested that TMN protein family members interact with cargo proteins with this specific domain to transport them to the cell surface. Immunoprecipitation analysis has shown that TM9SF4 physically interacts with the ATP6V1H subunit of V-ATPase to promote assembly of the V0/V1 sectors within the proton pump of HCT116 colon cancer cells (Lozupone *et al.*, 2015). Therefore, *TM9SF4* silencing caused a reduction in V-ATPase activity associated with alkalinization of intracellular acidic vesicles required for colon cancer cell invasion. In addition, TM9SF4 was localized to the Golgi, endosome compartments, and autophagosome in HEK293 cells; *TM9SF4* knockdown led to reduction of autophagic flux induced by nutrient starvation (Sun *et al.*, 2018). These results suggest that the human TMN family is involved in cargo loading into intracellular vesicles, presumably by regulating V-ATPase activity.

In the current study, it was found that Arabidopsis TMN1 controls RG-II and RG-I deposition in the apoplast and that a major portion of TMN1 displayed the pattern of Golgi-localized proteins. The cytoplasmic tail of the C-terminus in AtTMN1

possesses the KXD/E motif, a Golgi retention signal, which is conserved among other TMN homologs in eukaryotes (Gao *et al.*, 2014). Furthermore, AtTMN1 interacts with Sec21 (a coat protein complex I subunit) and Sec24 (a coat protein complex II subunit) to mediate retrograde and anterograde transport, respectively, between the Golgi apparatus and endoplasmic reticulum (Gao *et al.*, 2012); thus, AtTMN1 is presumably involved in a vesicular trafficking system. Given the Golgi localization of a series of proteins, including glycosyltransferases and nucleotide sugar transporters required for pectin biosynthesis (Mohnen, 2008; Nikolovski *et al.*, 2012), and the interaction of AtTMN1 with coat protein complex subunits, AtTMN1 may transport these proteins required for RG-II and RG-I synthesis from the endoplasmic reticulum to the Golgi. On the other hand, it is not ruled out a possibility that Arabidopsis TMN1 is involved in trafficking of biosynthesized pectin from the Golgi to apoplast, considering that ECHIDNA, YPT/RAB GTPase interacting Protein 4a and b are localized on the *trans*-Golgi network but not plasma membrane; they function in secretion of HG, RG-I and xyloglucan (Gendre *et al.*, 2013; McFarlane *et al.*, 2013). Therefore, it is possible that a minor portion of AtTMN1 localized at the *trans*-Golgi network contributes to pectin transport.

In conclusion, the results of this study demonstrate that the plant TMN family plays roles in RG-II and RG-I pectic polysaccharide deposition for normal cell elongation and cellular attachment. It was also found that the pectin synthesis mutant exhibited reduced sensitivity to low B supply in terms of cell elongation. The findings shed light on the mechanisms of growth regulation, which are dependent on changes in pectin content under low B conditions. This thesis provides a novel insight into mechanisms underlying pectin synthesis required for plant growth and development as multicellular organisms.

5. Acknowledgements

First and foremost, I greatly appreciate Dr. Kyoko Miwa who had endowed me with knowledge to perform my research. Thanks to her great guidance, I had achieved my goal of academics.

I sincerely express my appreciation to Dr. Shingo Sakamoto and Dr. Nobutaka Mitsuda (National Institute of Advanced Industrial Science and Technology (AIST)) for collaboration in this work, especially in measurement of sugar composition analysis.

I would like to express my gratitude to Prof. Masaaki Morikawa, Prof. Yoshifumi Yamaguchi, Prof. Ken-ichi Yamazaki and Prof. Tomomichi Fujita for kind encouragement and valuable discussions as referees in my Ph.D. defense.

I am grateful to Hiroko Yamamoto (Hokkaido University) for helpful instruction on equipment. I give special thanks to Toshiaki Ito and Dr. Masanori Yasui (Hokkaido University) for technical assistance with an ultramicrotome and a confocal laser scanning microscope at Electron Microscope Laboratory in Research Faculty of Agriculture. I thank Dr. Toshihiro Watanabe (Hokkaido University) for assistance in ICP-MS. I thank Dr. Masaru Kobayashi (Kyoto University) for providing the RG-II antibody.

I sincerely am grateful to the all members of Miwa laboratory and Course of Molecular Biology, Graduate School of Environmental Science for discussion or technical supports.

6. References

Ahn JW, **Verma R**, **Kim M**, **Lee JY**, **Kim YK**, **Bang JW**, **Reiter WD**, **Pai HS**. 2006. Depletion of UDP-D-apiose/UDP-D-xylose synthases results in rhamnogalacturonan-II deficiency, cell wall thickening, and cell death in higher plants. Journal of Biological Chemistry **281,** 13708–13716.

Bennett T, **van den Toorn A**, **Sanchez-Perez GF**, **Campilho A**, **Willemsen V**, **Snel B**, **Scheres B**. 2010. SOMBRERO, BEARSKIN1, and BEARSKIN2 regulate root cap maturation in *Arabidopsis*. The Plant Cell **22,** 640–654.

Bergeret E, **Perrin J**, **Williams M**, **Grunwald D**, **Engel E**, **Thevenon D**, **Taillebourg E**, **Bruckert F**, **Cosson P**, **Fauvarque MO**. 2008. TM9SF4 is required for *Drosophila* cellular immunity via cell adhesion and phagocytosis. Journal of Cell Science **121,** 3325–3334.

Bouton S, **Leboeuf E**, **Mouille G**, **Leydecker MT**, **Talbotec J**, **Granier F**, **Lahaye M**, **Höfte H**, **Truong HN**. 2002. QUASIMODO1 encodes a putative membrane-bound glycosyltransferase required for normal pectin synthesis and cell adhesion in Arabidopsis. The Plant Cell **14,** 2577–2590.

Camacho-Cristóbal JJ, **Martín-Rejano EM**, **Herrera-Rodríguez MB**, **Navarro-Gochicoa MT**, **Rexach J**, **González-Fontes A**. 2015. Boron deficiency inhibits root cell elongation via an ethylene/auxin/ROS-dependent pathway in *Arabidopsis* seedlings. Journal of Experimental Botany **66,** 3831–3840.

Chatterjee M, **Tabi Z**, **Galli M**, **Malcomber S**, **Buck A**, **Muszynski M**, **Gallavotti A**. 2014. The boron efflux transporter ROTTEN EAR is required for maize inflorescence development and fertility. The Plant Cell **26,** 2962–2977.

Clough SJ, **Bent AF**. 1998. Floral dip: a simplified method for *Agrobacterium*-mediated transformation of *Arabidopsis thaliana*. The Plant Journal **16**, 735–743

Cornillon S, **Pech E**, **Benghezal M**, **Ravanel K**, **Gaynor E**, **Letourneur F**, **Brückert F**, **Cosson P**. 2000. Phg1p is a nine-transmembrane protein superfamily

member involved in *Dictyostelium* adhesion and phagocytosis. Journal of Biological Chemistry **275,** 34287–34292.

Cullen PJ, **Sprague GF** Jr. 2012. The regulation of filamentous growth in yeast. Genetics **190,** 23–49.

Curtis MD, **Grossniklaus U**. 2003. A Gateway cloning vector set for high-throughput functional analysis of genes in planta. Plant Physiology **133,** 462–469.

Daher FB, **Braybrook SA**. 2015. How to let go: pectin and plant cell adhesion. Frontiers in Plant Science **6,** 523.

Dell B, Huang LB. 1997. Physiological response of plants to low boron. Plant and Soil 193, 103–120.

Delmas F, **Séveno M**, **Northey JG**, **Hernould M**, **Lerouge P**, **McCourt P**, **Chevalier C**. 2008. The synthesis of the rhamnogalacturonan II component 3-deoxy-D-manno-2-octulosonic acid (Kdo) is required for pollen tube growth and elongation. Journal of Experimental Botany **59,** 2639–2647.

Dolan L, Janmaat K, Willemsen V, Linstead P, Poethig S, Roberts K, Scheres B. 1993. Cellular organisation of the *Arabidopsis thaliana* root. Development 119, 71–84.

Driouich A, **Follet-Gueye ML**, **Bernard S**, **Kousar S**, **Chevalier L**, **Vicré-Gibouin M**, **Lerouxel O**. 2012. Golgi-mediated synthesis and secretion of matrix polysaccharides of the primary cell wall of higher plants. Frontiers in Plant Science **3,** 79.

Durand C, **Vicré-Gibouin M**, **Follet-Gueye ML**, **Duponchel L**, **Moreau M**, **Lerouge P**, **Driouich A**. 2009. The organization pattern of root border-like cells of Arabidopsis is dependent on cell wall homogalacturonan. Plant Physiology **150,** 1411–1421.

Feng W, Kita D, Peaucelle A, Cartwright HN, Doan V, Duan Q, Liu MC, Maman J, Steinhorst L, Schmitz-Thom I, ***et al.*** 2018. The FERONIA receptor kinase maintains cell-wall integrity during salt stress through Ca^{2+} signaling. Current Biology 28, 666–675.

Froquet R, **Cherix N**, **Birke R**, **Benghezal M**, **Cameroni E**, **Letourneur F**, **Mösch HU**, **De Virgilio C**, **Cosson P**. 2008. Control of cellular physiology by TM9 proteins in yeast and *Dictyostelium*. Journal of Biological Chemistry **283,** 6764–6772.

Froquet R, **le Coadic M**, **Perrin J**, **Cherix N**, **Cornillon S**, **Cosson P**. 2012. TM9/Phg1 and SadA proteins control surface expression and stability of SibA adhesion molecules in *Dictyostelium*. Molecular Biology of the Cell **23,** 679–686.

Fujiwara T, **Hirai MY**, **Chino M**, **Komeda Y**, **Naito S**. 1992. Effects of sulfur nutrition on expression of the soybean seed storage protein genes in transgenic petunia. Plant Physiology **99,** 263–268.

Gao C, **Cai Y**, **Wang Y**, **Kang BH**, **Aniento F**, **Robinson DG**, **Jiang L**. 2014. Retention mechanisms for ER and Golgi membrane proteins. Trends in Plant Science **19,** 508–515.

Gao C, **Yu CK**, **Qu S**, **San MW**, **Li KY**, **Lo SW**, **Jiang L**. 2012. The Golgi-localized *Arabidopsis* endomembrane protein12 contains both endoplasmic reticulum export and Golgi retention signals at its C terminus. The Plant Cell **24,** 2086–2104.

Gendre D, **McFarlane HE**, **Johnson E**, **Mouille G**, **Sjödin A**, **Oh J**, **Levesque-Tremblay G**, **Watanabe Y**, **Samuels L**, **Bhalerao RP**. 2013. *Trans*-Golgi network localized ECHIDNA/Ypt interacting protein complex is required for the secretion of cell wall polysaccharides in *Arabidopsis*. The Plant Cell **25,** 2633–2646.

Hegelund JN, **Jahn TP**, **Baekgaard L**, **Palmgren MG**, **Schjoerring JK**. 2010. Transmembrane nine proteins in yeast and *Arabidopsis* affect cellular metal contents without changing vacuolar morphology. Physiologia Plantarum **140,** 355–367.

Huang LB, Pant J, Dell B, Bell RW. 2000. Effects of boron deficiency on anther development and floret fertility in wheat (*Triticum aestivum* L-'Wilgoyne'). Annals of Botany 85, 493–500.

Ishii T, **Matsunaga T**, **Hayashi N**. 2001. Formation of rhamnogalacturonan II-borate dimer in pectin determines cell wall thickness of pumpkin tissue. Plant Physiology **126,** 1698–1705.

Iwai H, **Masaoka N**, **Ishii T**, **Satoh S**. 2002. A pectin glucuronyltransferase gene is essential for intercellular attachment in the plant meristem. Proceedings of the National Academy of Sciences, USA **99,** 16319–16324.

Kamiya M, Higashio SY, Isomoto A, Kim JM, Seki M, Miyashima S, Nakajima K. 2016. Control of root cap maturation and cell detachment by BEARSKIN transcription factors in *Arabidopsis*. Development 143, 4063–4072.

Kobayashi M, **Kouzu N**, **Inami A**, **Toyooka K**, **Konishi Y**, **Matsuoka K**, **Matoh T**. 2011. Characterization of Arabidopsis CTP:3-deoxy-D-manno-2-octulosonate cytidylyltransferase (CMP-KDO synthetase), the enzyme that activates KDO during rhamnogalacturonan II biosynthesis. Plant & Cell Physiology **52,** 1832–1843.

Kumar N, Iyer-Pascuzzi AS. 2020. Shedding the last layer: Mechanisms of root cap cell release. Plants (Basel) 9, 308.

Liu XL, Liu L, Niu QK, Xia C, Yang KZ, Li R, Chen LQ, Zhang XQ, Zhou Y, Ye D. 2011. *Male gametophyte defective 4* encodes a rhamnogalacturonan II xylosyltransferase and is important for growth of pollen tubes and roots in Arabidopsis. The Plant Journal 65, 647–660.

Lozupone F, Borghi M, Marzoli F, Azzarito T, Matarrese P, Iessi E, Venturi G, Meschini S, Canitano A, Bona R, Cara A, Fais S. 2015. TM9SF4 is a novel V-ATPase-interacting protein that modulates tumor pH alterations associated with drug resistance and invasiveness of colon cancer cells. Oncogene 34, 5163-5174.

Lozupone F, Perdicchio M, Brambilla D, Borghi M, Meschini S, Barca S, Marino ML, Logozzi M, Federici C, Iessi E, de Milito A, Fais S. 2009. The human homologue of Dictyostelium discoideum phg1A is expressed by human metastatic melanoma cells. EMBO reports 10, 1348-1354.

Matsunaga T, Ishii T. 2006. Borate cross-linked/total rhamnogalacturonan II ratio in cell walls for the biochemical diagnosis of boron deficiency in hydroponically grown pumpkin. Analytical Science 22, 1125–1127.

McFarlane HE, **Watanabe Y**, **Gendre D**, **Carruthers K**, **Levesque-Tremblay G**, **Haughn GW**, **Bhalerao RP**, **Samuels L**. 2013. Cell wall polysaccharides are mislocalized to the vacuole in echidna mutants. Plant & Cell Physiology **54,** 1867–1880.

Mohnen D. 2008. Pectin structure and biosynthesis. Current Opinion in Plant Biology **11,** 266–277.

Mösch HU, **Fink GR**. 1997. Dissection of filamentous growth by transposon mutagenesis in *Saccharomyces cerevisiae*. Genetics **145,** 671–684.

Nagasaki H, Mochizuki T, Kodama Y, et al. 2013. DDBJ read annotation pipeline: a cloud computing-based pipeline for high-throughput analysis of next-generation sequencing data. DNA Research **20**, 383–390.

Naramoto S, **Otegui MS**, **Kutsuna N**, ***et al.*** 2014. Insights into the localization and function of the membrane trafficking regulator GNOM ARF-GEF at the Golgi apparatus in *Arabidopsis*. The Plant Cell **26,** 3062–3076.

Nikolovski N, **Rubtsov D**, **Segura MP**, **Miles GP**, **Stevens TJ**, **Dunkley TP**, **Munro S**, **Lilley KS**, **Dupree P**. 2012. Putative glycosyltransferases and other plant Golgi apparatus proteins are revealed by LOPIT proteomics. Plant Physiology **160,** 1037–1051.

Nissen KS, **Willats WGT**, **Malinovsky FG**. 2016. Understanding CrRLK1L function: cell walls and growth control. Trends in Plant Science **21,** 516–527.

O'Neill MA, Eberhard S, Albersheim P, Darvill AG. 2001. Requirement of borate cross-linking of cell wall rhamnogalacturonan II for *Arabidopsis* growth. Science 294, 846–849.

O'Neill MA, **Ishii T**, **Albersheim P**, **Darvill AG**. 2004. Rhamnogalacturonan II: structure and function of a borate cross-linked cell wall pectic polysaccharide. Annual Review of Plant Biology **55,** 109–139.

Oomen RJ, **Doeswijk-Voragen CH**, **Bush MS**, ***et al.*** 2002. *In muro* fragmentation of the rhamnogalacturonan I backbone in potato (*Solanum tuberosum* L.) results in a reduction and altered location of the galactan and arabinan side-chains and abnormal periderm development. The Plant Journal **30,** 403–413.

Paolillo R, **Spinello I**, **Quaranta MT**, **Pasquini L**, **Pelosi E**, **Lo Coco F**, **Testa U**, **Labbaye C**. 2015. Human TM9SF4 is a new gene down-regulated by hypoxia and involved in cell adhesion of leukemic cells. PLoS One **10,** e0126968.

Perrin J, **Le Coadic M**, **Vernay A**, **Dias M**, **Gopaldass N**, **Ouertatani-Sakouhi H**, **Cosson P**. 2015a. TM9 family proteins control surface targeting of glycine-rich transmembrane domains. Journal of Cell Science **128,** 2269–2277.

Perrin J, **Mortier M**, **Jacomin AC**, **Viargues P**, **Thevenon D**, **Fauvarque MO**. 2015b. The nonaspanins TM9SF2 and TM9SF4 regulate the plasma membrane localization and signalling activity of the peptidoglycan recognition protein PGRP-LC in *Drosophila*. Journal of Innate Immunity **7,** 37–46.

Reboul R, **Geserick C**, **Pabst M**, **Frey B**, **Wittmann D**, **Lütz-Meindl U**, **Léonard R**, **Tenhaken R**. 2011. Down-regulation of UDP-glucuronic acid biosynthesis leads to swollen plant cell walls and severe developmental defects associated with changes in pectic polysaccharides. Journal of Biological Chemistry **286,** 39982–39992.

Robinson D, Jiang L, Schumacher K. 2008. The endosomal system of plants: charting new and familiar territories. Plant Physiology **147**, 1482–1492.

Sakamoto S, Yoshida K, Sugihara S, Mitsuda N. 2015. Development of a new high-throughput method to determine the composition of ten monosaccharides

including 4-*O*-methyl glucuronic acid from plant cell walls using ultra-performance liquid chromatography. Plant Biotechnology 32, 55–63.

Sechet J, **Htwe S**, **Urbanowicz B**, ***et al.*** 2018. Suppression of Arabidopsis GGLT1 affects growth by reducing the L-galactose content and borate cross-linking of rhamnogalacturonan-II. The Plant Journal **96,** 1036–1050.

Sinclair R, **Rosquete MR**, **Drakakaki G**. 2018. Post-Golgi trafficking and transport of cell wall components. Frontiers in Plant Science **9,** 1784.

Sun L, Meng Z, Zhu Y, Lu J, Li Z, Zhao Q, Huang Y, Jiang L, Yao X. 2018. TM9SF4 is a novel factor promoting autophagic flux under amino acid starvation. Cell Death and Differentiation 25, 368-379.

Voragen AGJ, Coenen G-J, Verhoef RP, Schols HA. 2009. Pectin, a versatile polysaccharide present in plant cell walls. Structural Chemistry 20, 263–275.

Voxeur A, **Gilbert L**, **Rihouey C**, **Driouich A**, **Rothan C**, **Baldet P**, **Lerouge P**. 2011. Silencing of the GDP-D-mannose 3,5-epimerase affects the structure and cross-linking of the pectic polysaccharide rhamnogalacturonan II and plant growth in tomato. Journal of Biological Chemistry **286,** 8014–8020.

Wang Q, **Lu L**, **Wu X**, **Li Y**, **Lin J**. 2003. Boron influences pollen germination and pollen tube growth in *Picea meyeri*. Tree Physiology **23,** 345–351.

Warington K. 1933. The Influence of length of day on the response of plants to boron. Annals of Botany os-47, 429–458.

Winter D, **Vinegar B**, **Nahal H**, **Ammar R**, **Wilson GV**, **Provart NJ**. 2007. An “Electronic Fluorescent Pictograph” browser for exploring and analyzing large-scale biological data sets. PLoS One **2,** e718.

York WS, **Darvill AG**, **McNeil M**, **Albersheim P**. 1985. 3-Deoxy-D-manno-2-octulosonic acid (KDO) is a component of rhamnogalacturonan II, a pectic polysaccharide in the primary cell walls of plants. Carbohydrate Research 138, 109–126.

Zhou T, **Hua Y**, **Zhang B**, **Zhang X**, **Zhou Y**, **Shi L**, **Xu F**. 2017. Low-boron tolerance strategies involving pectin-mediated cell wall mechanical properties in *Brassica napus*. Plant & Cell Physiology **58,** 1991–2005.

Zhou Y, **Kobayashi M**, **Awano T**, **Matoh T**, **Takabe K**. 2018. A new monoclonal antibody against rhamnogalacturonan II and its application to immunocytochemical detection of rhamnogalacturonan II in Arabidopsis roots. Bioscience, Biotechnology, and Biochemistry **82,** 1780–1789.

7. List of publications

Hiroguchi A, Sakamoto S, Mitsuda N, Miwa K. (2021). Golgi-localized membrane protein AtTMN1/EMP12 functions in the deposition of rhamnogalacturonan II and I for cell growth in Arabidopsis. Journal of Experimental Botany. **72**: 3611-3629. **doi: 10.1093/jxb/erab065**

Table 1. F2 segregating population derived from F1 of mutants nos.19 or 45 crossed with L*er*.

Plants were grown on solid media under 0.03 μM B condition for 11-13 d under long-day conditions. The number of plants showing increased PR elongation compared to Col-0 or similar PR lengths to Col-0 was counted.

F1 genotype	The number of plants with mutant phenotypes	The numbers of plants similar to Col-0	Total numbers of germinated F2 population
No.19/ L*er*	26	106	132
No.45/ L*er*	51	294	345

Table 2. No reduction in the relative proportion of RG-II-B dimer formation in the *tmn1* mutants.

Relative proportions of RG-II-B dimer in rosette leaf and root cell walls of Col-0, *tmn1-1*, *tmn1-2* and *tmn1-3*. The plants were grown hydroponically under 0.1 μM, 0.3 μM, 100 μM, and 500 μM B for 44 d under short days. For one individual cell wall sample, six plants for rosette leaves and roots were harvested to be homogenized. RG-II-B dimers and RG-II monomers released from AIRs by EPG were detected by size-exclusion HPLC/refractive index detector. Relative proportions represent percentages of RG-II-B dimer peak area which is divided by total area of RG-II-B dimers and RG-II monomers. Values represent means ± SD from three and four independent cell wall samples for rosette leaves and roots, respectively. The value of *tmn1-3* rosette leaf under 0.3 μM B represents a mean from two independent cell wall samples. Significant differences between Col-0 and the *tmn1* mutants under each B condition are indicated as **P*<0.05, ***P*<0.01 (Dunnett's multiple comparison test). AIR, alcohol-insoluble residue. Please clarify – relative proportion as a percentage of what? Please state how this percentage was calculated.

	Relative proportion of RG-II-B dimer in rosette leaf (%)				Relative proportion of RG-II-B dimer in root (%)			
Plant line	0.1 μM B in media	0.3 μM B in media	100 μM B in media	500 μM B in media	0.1 μM B in media	0.3 μM B in media	100 μM B in media	500 μM B in media
Col-0	78.0 ± 3.5	85.9 ± 1.5	91.1 ± 5.5	93.8 ± 1.7	62.1 ± 4.2	72.2 ± 3.2	92.5 ± 0.4	90.4 ± 4.1
tmn1-1	86.8 ± 3.8*	84.6 ± 3.7 *	87.8 ± 2.0	91.3 ± 2.2	71.3 ± 5.8	81.7 ± 1.9**	90.7 ± 2.6	95.0 ± 0.4
tmn1-2	85.1 ± 1.8*	89.0 ± 0.6	89.9 ± 2.7	91.9 ± 2.1	73.8 ± 4.5	83.5 ± 3.2**	92.9 ± 3.3	93.3 ± 3.7
tmn1-3	85.6 ± 2.3*	89.5	91.9 ± 2.2	91.9 ± 3.6	75.3 ± 6.2*	82.8 ± 1.2**	90.9 ± 2.1	92.7 ± 0.3

Table 3. Reduced rhamnose contents in *tmn1* mutant cell walls treated with amylase.

The 10 monosaccharides contents were determined in rosette leaf cell walls treated with amylase. The molar percentages were calculated by dividing with total detected monosaccharide contents. Plants were grown hydroponically under 100 µM B for 44 d under short days. Rosette leaves of six plants were harvested and homogenized to create one independent cell wall sample. After amylase treatment, the quantities of 10 monosaccharides were determined. Data are means ± SD from four independent rosette leaf cell walls treated with amylase in Col-0, *tmn1-1*, *tmn1-2*, and *tmn1-3*. Asterisks indicate significant differences between Col-0 and the *tmn1* mutants (**P*<0.05, ***P*<0.01, ****P*<0.001; Dunnett's multiple comparison test). Rha, L-rhamnose; GalA, D-galacturonic acid; Glc, D-glucose; Xyl, D-xylose; Man, D-mannose; Ara, L-arabinose; Gal, D-galactose; Fuc, L-fucose; m-GlcA, 4-*O*-methyl-D-glucuronic acid; GlcA, D-glucuronic acid.

	Mol% of monosaccharides in rosette leaf cell wall									
Plant line	Rha	GalA	Glc	Xyl	Man	Ara	Gal	Fuc	mGlcA	GlcA
Col-0	7.75 ± 0.11	41.6 ± 0.67	24.2 ± 0.60	5.84 ± 0.07	1.91 ± 0.05	9.41 ± 0.23	7.63 ± 0.08	1.23 ± 0.02	0.27 ± 0.02	0.14 ± 0.01
tmn1-1	5.65 ± 0.14***	38.9 ± 1.12*	27.9 ± 0.74***	6.26 ± 0.17**	2.16 ± 0.12**	9.73 ± 0.22	7.48 ± 0.21	1.41 ± 0.05***	0.33 ± 0.06	0.20 ± 0.02***
tmn1-2	5.83 ± 0.13***	40.1 ± 1.75	27.7 ± 0.59***	6.22 ± 0.15**	2.13 ± 0.10*	8.99 ± 0.54	7.16 ± 0.37	1.33 ± 0.08*	0.32 ± 0.04	0.18 ± 0.01*
tmn1-3	5.80 ± 0.14***	40.9 ± 1.65	27.4 ± 0.57***	6.27 ± 0.08**	2.09 ± 0.07*	8.77 ± 0.61	7.04 ± 0.27*	1.30 ± 0.04	0.32 ± 0.18	0.17 ± 0.01*

Table 4. Reduced rhamnose and galacturonic acid contents in *tmn1* mutant cell walls without amylase treatment.
The 10 monosaccharides contents were determined in rosette leaf cell walls treated without amylase. The molar percentages were calculated by dividing with total detected monosaccharide contents. Plants were grown hydroponically under 100 μM B condition for 44 d under short-day conditions. Rosette leaves of six plants were harvested and homogenized to create one independent cell wall sample. The quantities of 10 monosaccharide were determined. Data are means ± SD from four independent rosette leaf cell walls in Col-0, *tmn1-1*, *tmn1-2* and *tmn1-3*. Asterisks indicate significant differences between Col-0 and the *tmn1* mutants (**P*<0.05, ***P*<0.01, ****P*<0.001; Dunnett's multiple comparison test). Rha, L-rhamnose; GalA, D-galacturonic acid; Glc, D-glucose; Xyl, D-xylose; Man, D-mannose; Ara, L-arabinose; Gal, D-galactose; Fuc, L-fucose; m-GlcA, 4-*O*-methyl-D-glucuronic acid; GlcA, D-glucuronic acid.

	Mol% of monosaccharides in rosette leaf cell wall									
Plant line	Rha	GalA	Glc	Xyl	Man	Ara	Gal	Fuc	mGlcA	GlcA
Col-0	6.27 ± 0.18	31.4 ± 1.18	38.6 ± 1.61	3.70 ± 0.10	2.03 ± 0.10	8.80 ± 0.25	7.67 ± 0.09	1.15 ± 0.04	0.17 ± 0.01	0.17 ± 0.02
tmn1-1	4.56 ± 0.18***	26.8 ± 2.08**	43.0 ± 2.01	3.91 ± 0.16	2.36 ± 0.13	9.71 ± 0.44	7.86 ± 0.25	1.41 ± 0.05***	0.29 ± 0.03**	0.17 ± 0.12
tmn1-2	4.94 ± 0.34***	26.0 ± 2.53**	45.8 ± 3.44**	3.36 ± 0.57	2.75 ± 0.30***	8.57 ± 0.36	6.92 ± 0.65*	1.30 ± 0.08**	0.27 ± 0.06**	0.07 ± 0.10
tmn1-3	4.57 ± 0.15***	29.4 ± 0.58	41.7 ± 1.81	4.06 ± 0.17	2.25 ± 0.08	8.74 ± 0.74	7.53 ± 0.32	1.27 ± 0.04*	0.19 ± 0.04	0.27 ± 0.09

Table 5. Primers used in this study

Primer ID	Stock No.	Name	Sequence (5' > 3')	Purpose
P1	609	*tmn1-1*_dCAPS_For	GCTGGTTTATTCAGGTAAACATCG	Genotyping of *tmn1-1*
P2	343	*tmn1-1*_dCAPS_Rev	AGGGAGACGACTGATGGAGT	
P3	692	*tmn1-2*_CAPS_For	ACCTTTGTGGGGTATGAACTT	Genotyping of *tmn1-2*
P4	693	*tmn1-2*_CAPS_Rev	TGCTTAATGGCGTGGTAACAA	
P5	348	WiscDsLoxHS_LB	TGATCCATGTAGATTTCCCGGACATGAAG	Genotyping of *tmn1-3*
P6	342	*TMN1*_genome_For	GCACAGGAACGGGATGTAAGT	
P7	343	*TMN1*_genome_Rev	AGGGAGACGACTGATGGAGT	
P8	354	*TMN1*_Coding sequence1_For	ATGCCGTCTTCCTCCTCCGCCG	Detection of full-length *TMN1* transcript
P9	359	*TMN1*_Coding sequence1_Rev	GTCGCACTTGATGTTTCTGTAG	
P10	849	*Actin1*_5' UTR_For	CTCCGATTTGATGGAGTCTGGT	Detection of full-length *Actin1* transcript
P11	850	*Actin1*_3' UTR_Rev	TGAAGAGGAAGAGGTGTGTACT	
P12	350	*TMN1*_Promoter1_For	CACCTTCAGACGTGGAGCAGGACT	Cloning of full-length *TMN1* genome
P13	351	*TMN1*_Terminater_Rev	CGATGTGTGGGCTCTTGTGT	
P14	353	*TMN1*_Promoter2_For	GCCTAAACAAACTCCCATCATG	Cloning of TMN1 signal peptide
P15	362	*TMN1*_N-terminus_Rev	ACCATAGAACCACCACCACCATCGGATGCGAACGTAGGAG	
P16	363	*GFP*_Coding sequence_For	CCGATGGTGGTGGTGGTTCTATGGTGAGCAAGGGCGAGGA	Cloning of *GFP* coding sequence
P17	364	*GFP*_Coding sequence_Rev	AGATCCTCCTCCTGATCCTCCTCCCTTGTACAGCTCGTCCATGC	
P18	365	*TMN1*_Coding sequence2_For	GGAGGAGGATCAGGAGGAGGATCTTCAGATCACAAGGTAAGACT	Cloning of *TMN1* coding sequence
P19	370	*TMN1*_Coding sequence2_Rev	CGAGAATCTCAAACCAACATC	

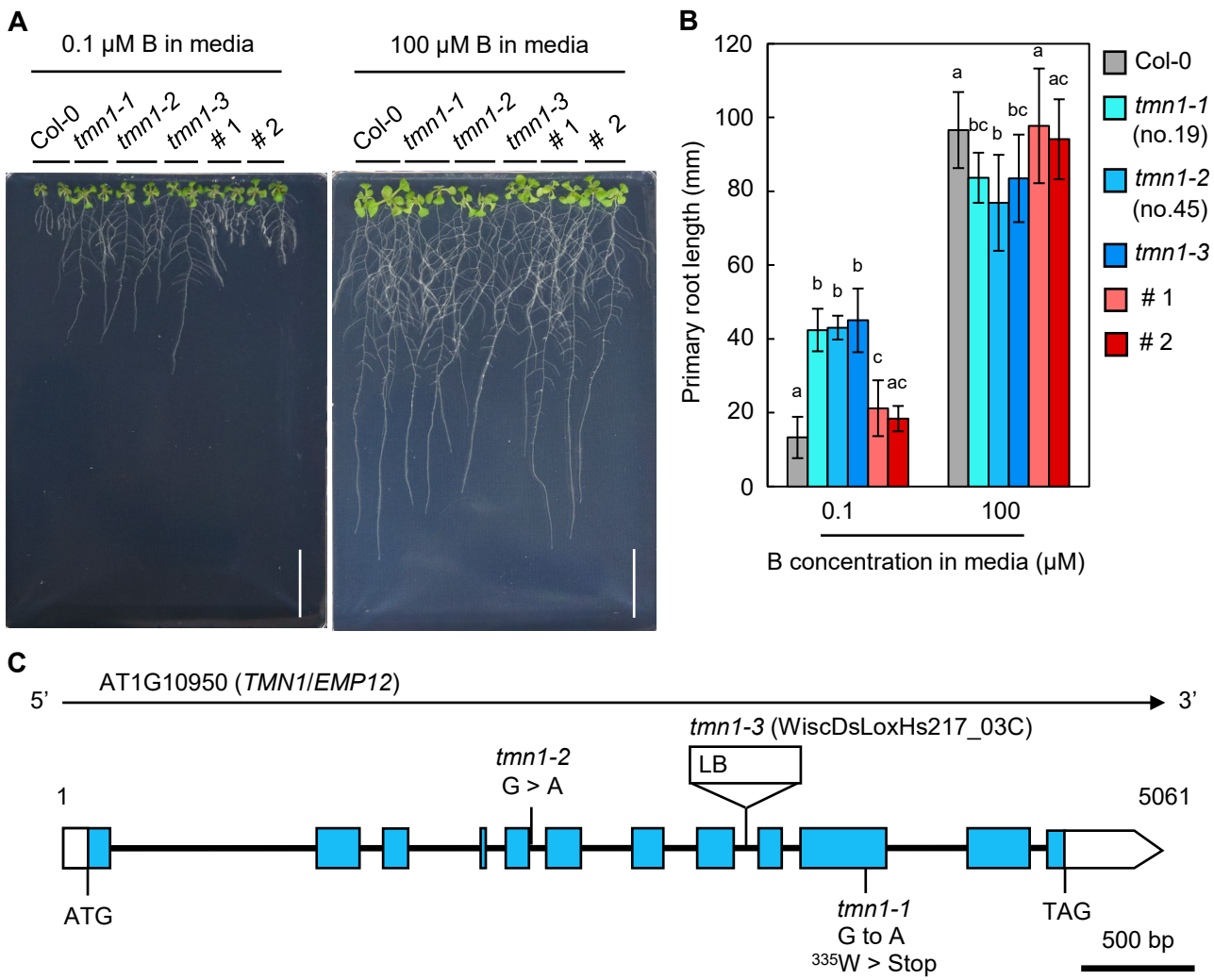

Figure 1. Impaired B nutrient response caused by loss of AtTMN1 function.
(A) Eleven DAS seedlings of Col-0, *tmn1-1* (no.19), *tmn1-2* (no.45), *tmn1-3*, and *tmn1-1* carrying *proAtTMN1:SP(AtTMN1)-GFP-AtTMN1genome* (lines #1 and #2) grown on solid media supplemented with 0.1 μM and 100 μM boric acid. Scale bars =20 mm. (B) Primary root lengths of seedlings 11 DAS under 0.1 μM and 100 μM B. Values are means ± SD of 16–20 individual plants. Different letters indicate significant differences among plant lines for each B condition (P<0.05, Tukey–Kramer test). (C) Gene structure of *AtTMN1* and mutation positions in *tmn1* alleles. Blue and white boxes indicate exons and untranslated regions, respectively. Black lines across exons indicate introns. Triangle indicates T-DNA insertion. Numbers correspond to the position of the genomic sequence from a transcriptional start site. (D) Insertion region of the fifth intron (81 bp) in *tmn1-2*. Uppercase and lowercase letters indicate exons and introns, respectively. A bold red letter represents a single-base substitution in *tmn1-2*. Numbers correspond to the position of the coding sequence from a translation start site. (E) *AtTMN1* transcripts (1.77 kb) amplified from cDNA in rosette leaves and roots using a *AtTMN1*-specific primer. *ACTIN1* full-length transcripts (1.69 kb) were amplified as a reference. M, DNA size marker.

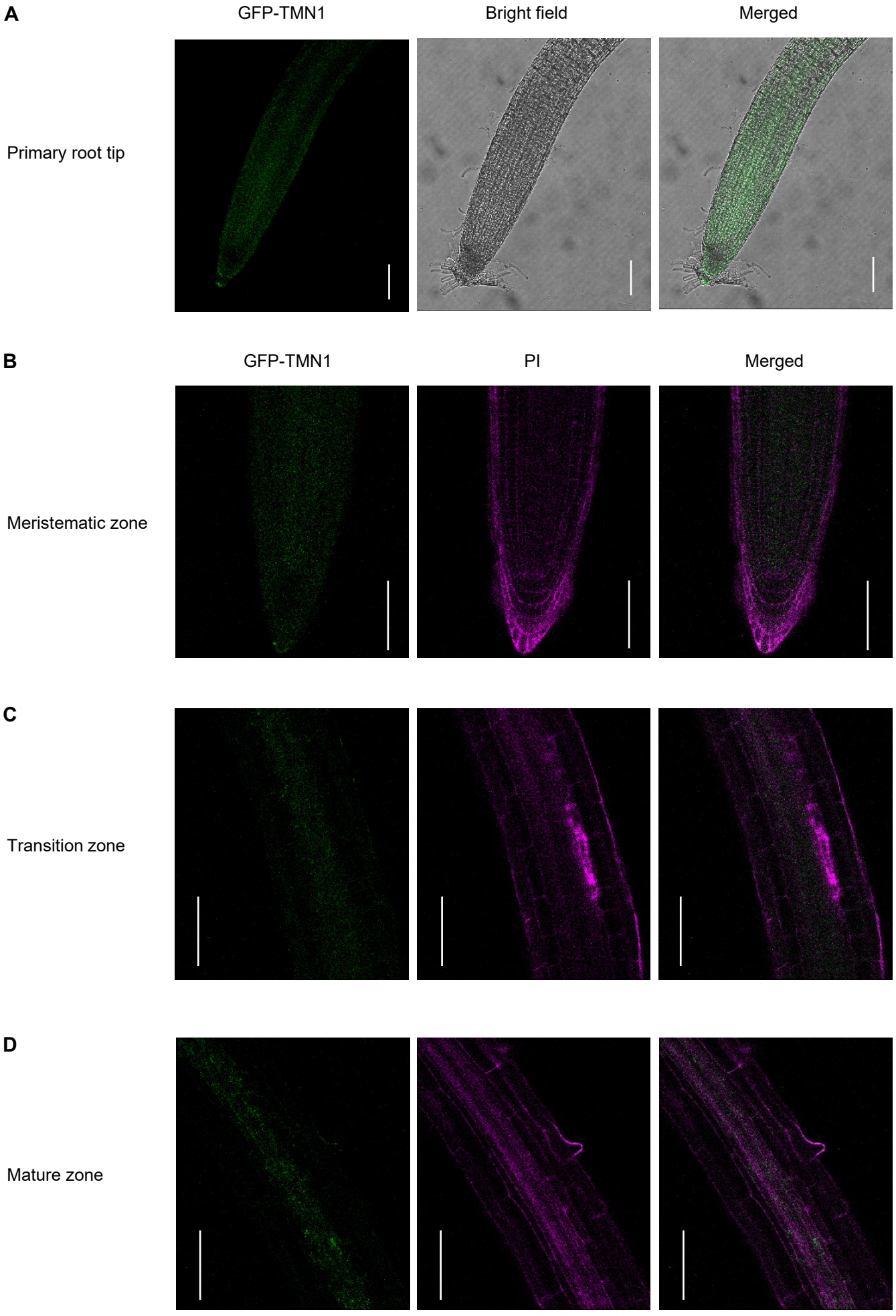

Figure 2. Expression of GFP-AtTMN1 in root tips.
Representative images of GFP-AtTMN1 fluorescence of root tip (A), meristematic zone (B), transition zone (C) and mature zone in PRs. Five-d-old transgenic plants carrying *proAtTMN1:SP(AtTMN1)-GFP-AtTMN1genome* (#1) under 100 μM B condition. Scale bars =100 μm. Their fluorescence in (B), (C) and (D) was enhanced using Leica Application Suite Advanced Fluorescence Lite.

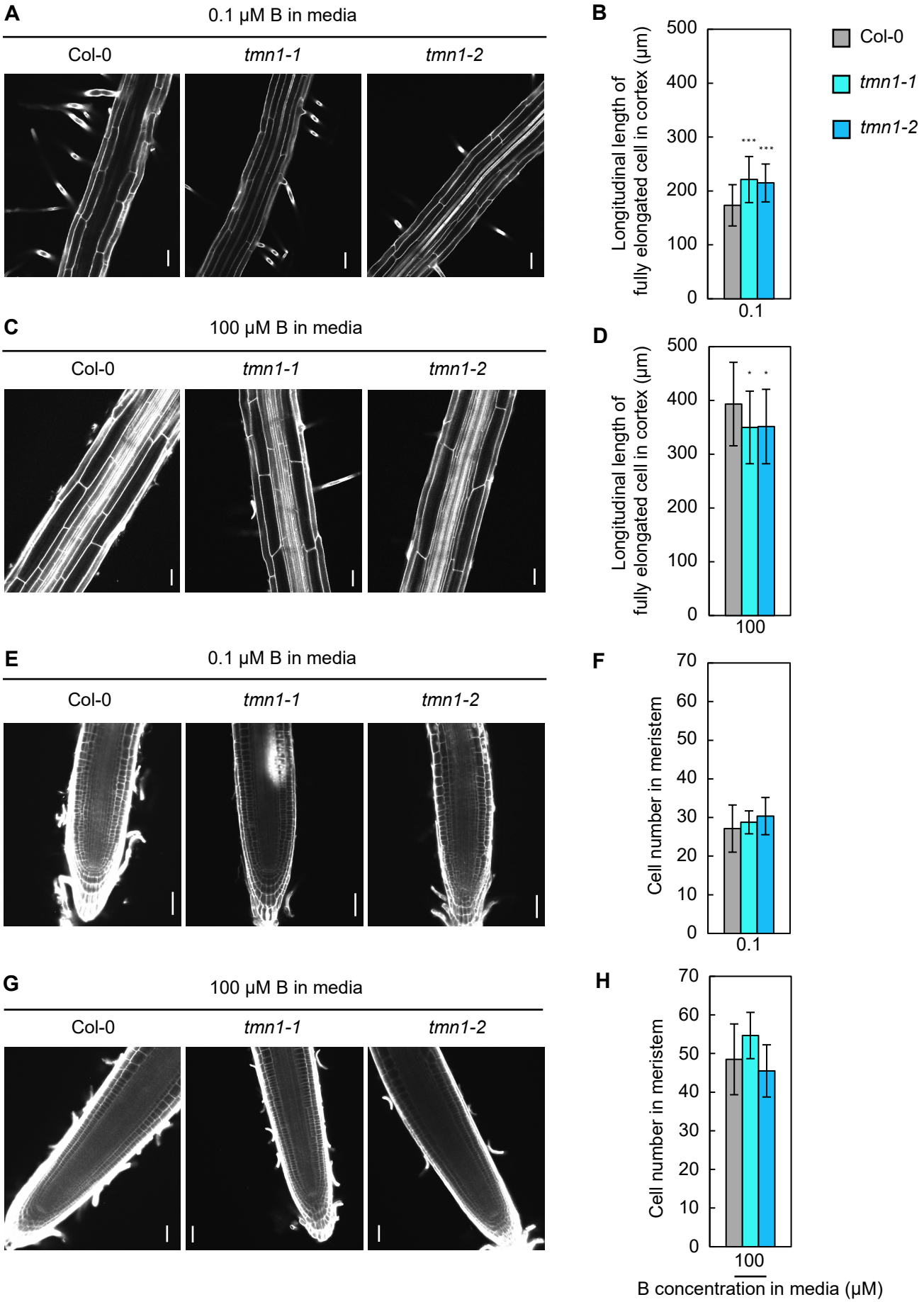

Figure 3. Increased and reduced cell elongation in the *tmn1* mutants under severely low and normal B conditions, respectively.

(A, C) Representative confocal images of mature root cells stained with PI and (B, D) longitudinal lengths of fully elongated cortical cells of Col-0, *tmn1-1*, and *tmn1-2* at four DAS under 0.1 μM B (A, B) and at 11 DAS under 100 μM B (C, D). Values are means ± SD from 29–67 independent cells in 10–19 individual plants. (E, G) Representative confocal images of root meristematic cells stained with PI and (F, H) cortical cell numbers between the quiescent centre and the first elongating cortical cell in seedlings of Col-0, *tmn1-1*, and *tmn1-2* at four DAS under 0.1 μM B (E, F) and at 11 DAS under 100 μM B (G, H). Values are means ± SD from six to 15 individual plants. Scale bars =50 μm. Asterisks indicate significant differences between Col-0 and the *tmn1* mutants (**P*<0.05, ****P*<0.001; Dunnett's multiple comparison test).

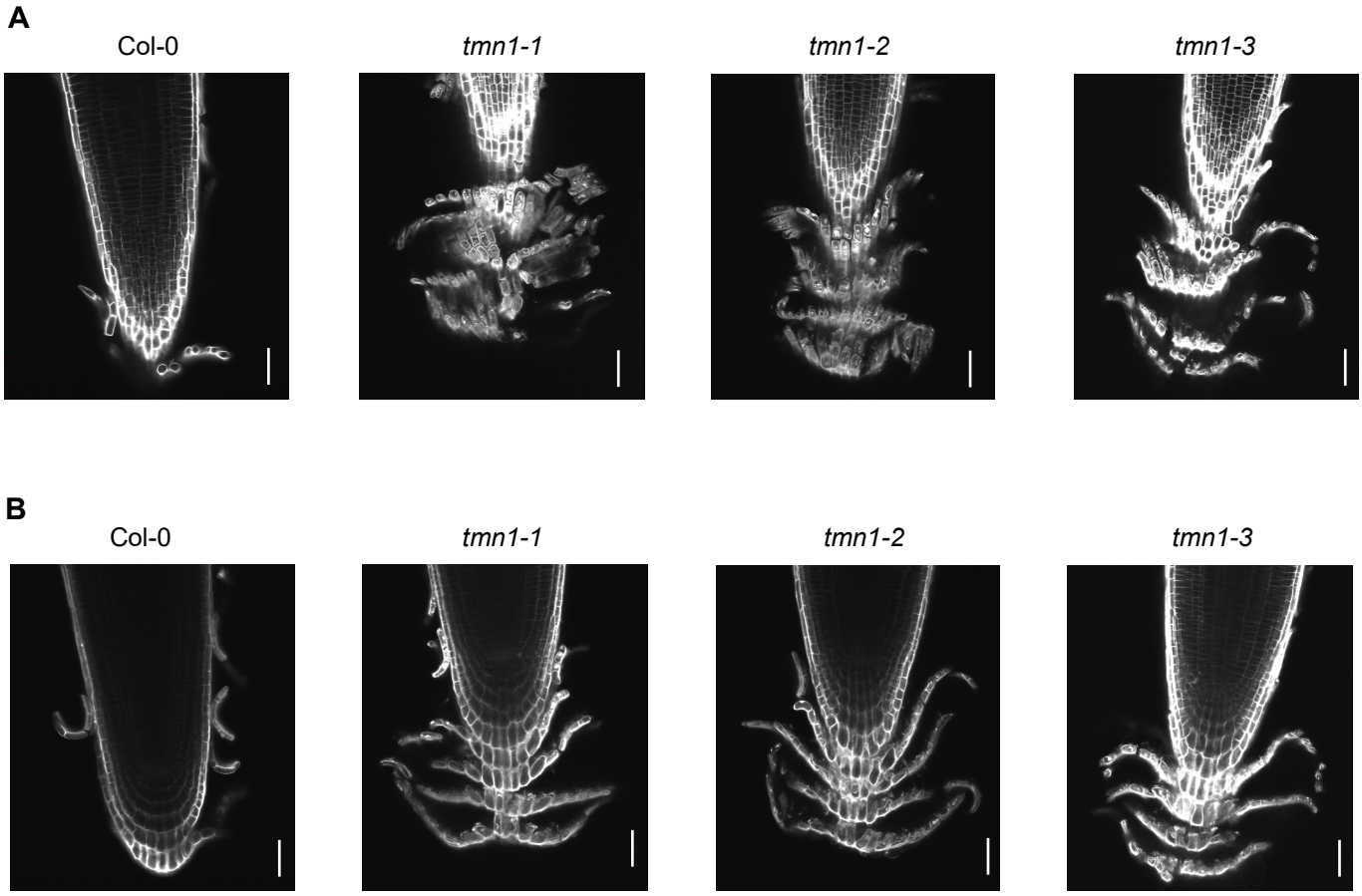

Figure 4. Failed cellular detachment of root caps in the *tmn1* mutants under sufficient B condition.
Representative confocal images taken at positions of root surface (A) and focusing on centre (B) in 14-d-old seedlings of Col-0, *tmn1-1*, *tmn1-2* and *tmn1-3* under 100 μM B condition. Roots stained with PI. Scale bars =50 μm.

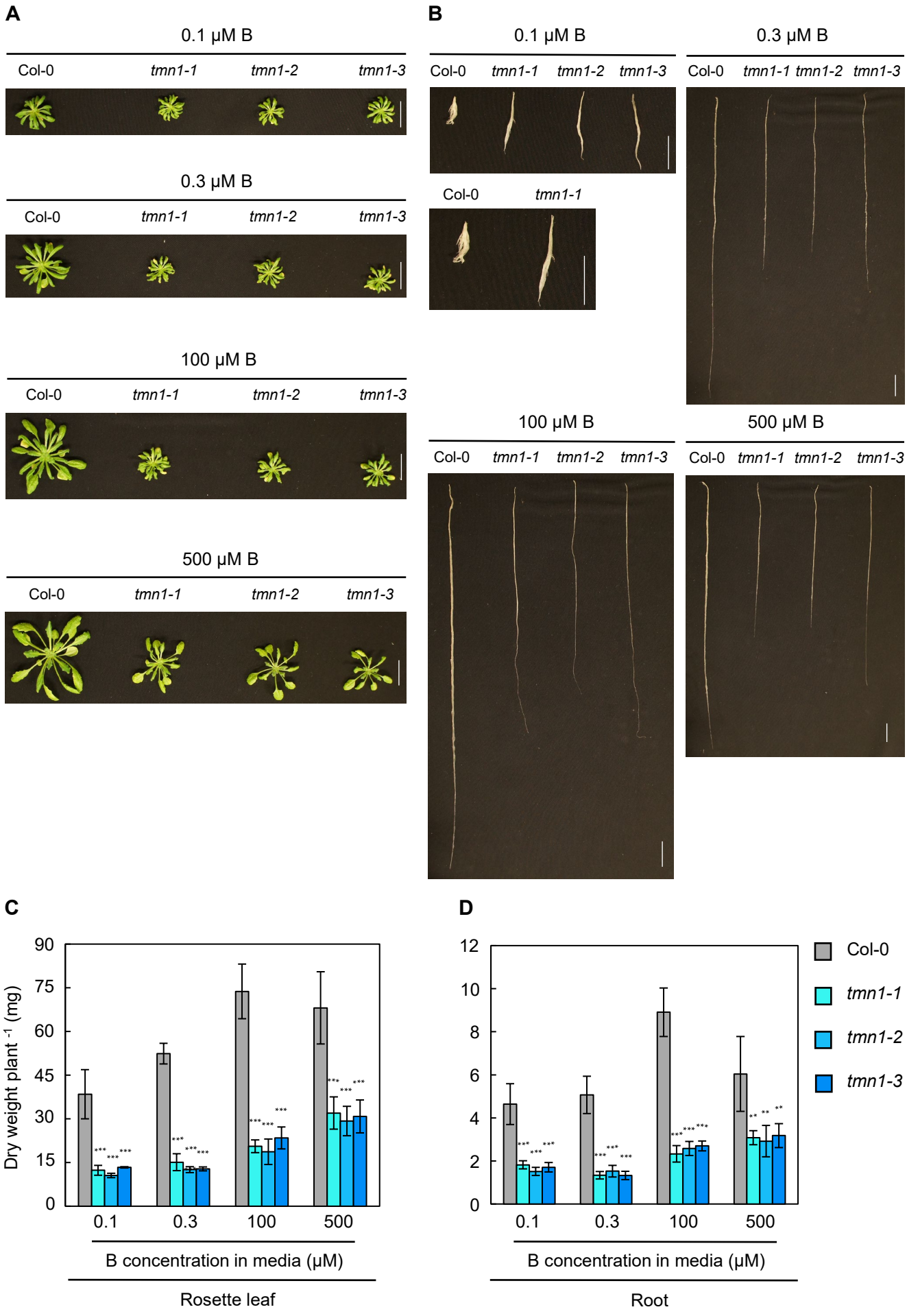

Figure 5. Defective vegetative growth in the *tmn1* mutants.
Rosette leaves (A) and roots (B) of Col-0, *tmn1-1*, *tmn1-2*, and *tmn1-3* plants grown hydroponically for 44 d under 0.1 μM, 0.3 μM, 100 μM, and 500 μM B treatments under short days. Scale bars =20 mm. Dry weights of rosette leaves (C) and roots (D) in Col-0, *tmn1-1*, *tmn1-2*, and *tmn1-3* grown for 45 d. Values are means ± SD from four independent plants. Asterisks indicate significant differences between Col-0 and the *tmn1* mutants under each B treatment (***P*<0.01, ****P*<0.001; Dunnett's multiple comparison test).

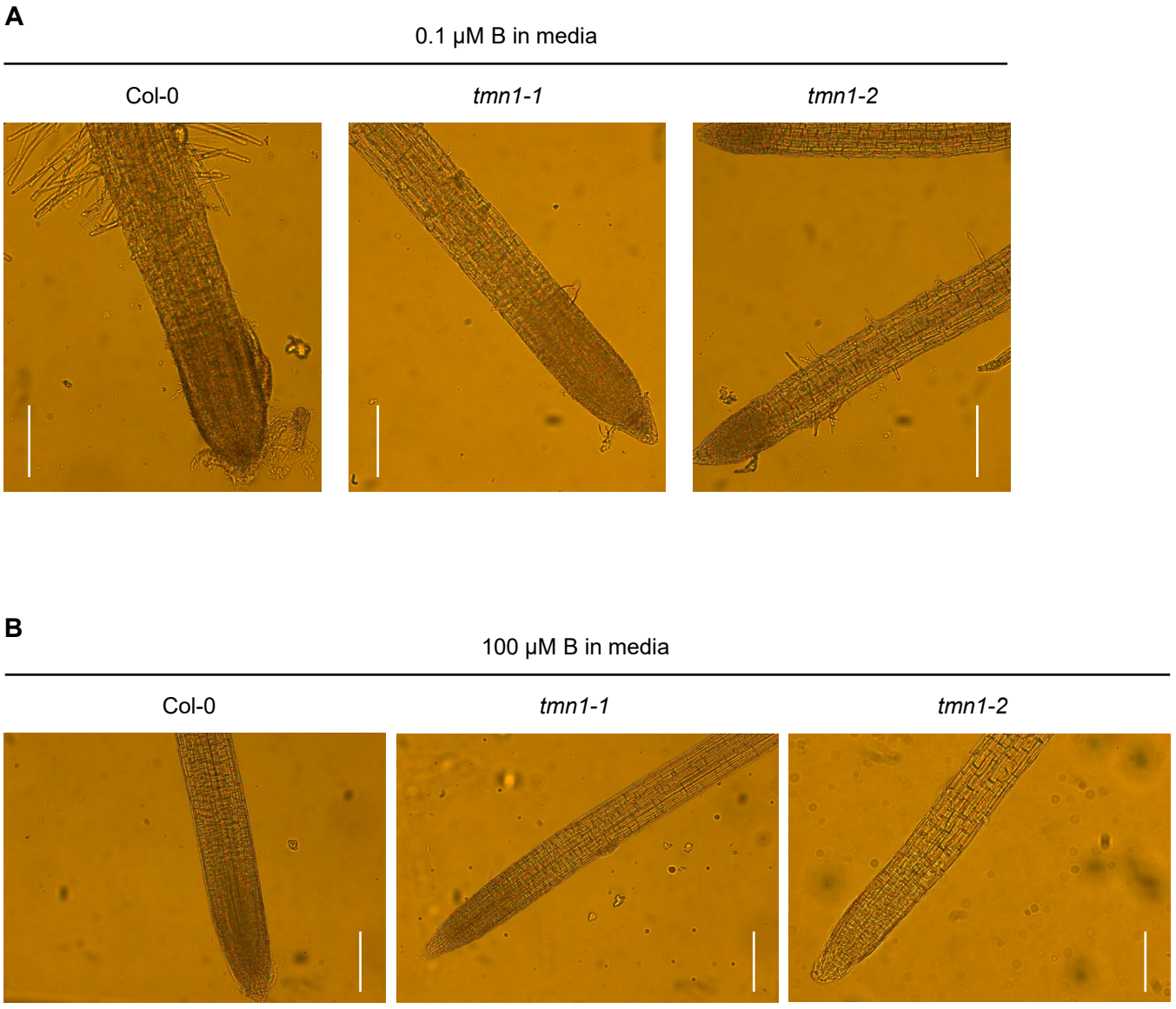

Figure 6. Reduction tendency of root tip thickness in *tmn1-1* and *tmn1-2*.
Root tip thickness of Col-0, *tmn1-1* and *tmn1-2*. The plants were grown hydroponically for 44 d under short-day conditions. The longest roots of each bundle were observed under 0.1 (A) and 100 μM B conditions. Bright field images were shown. Scale bars =100 μm.

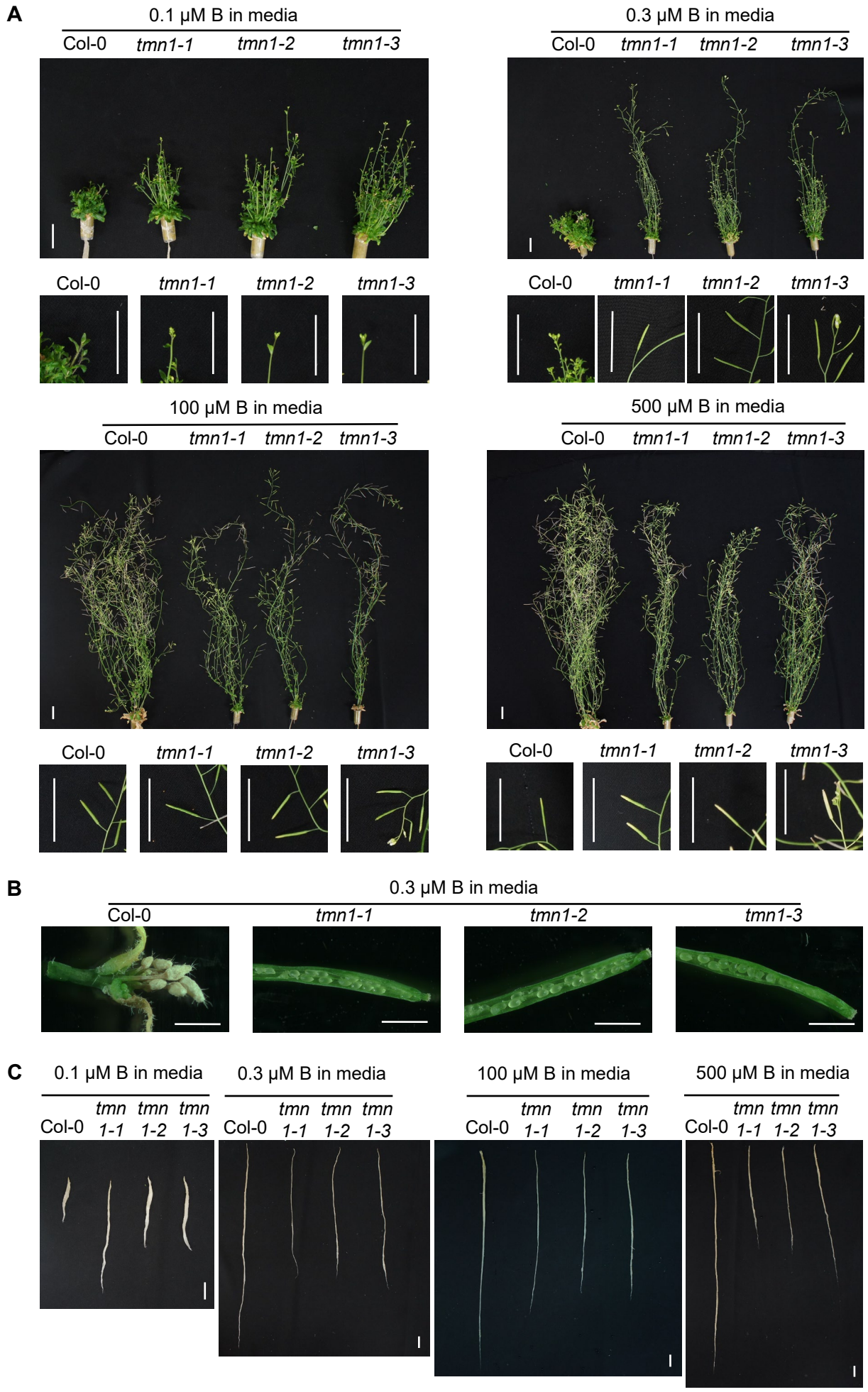

Figure 7. Restoration of *tmn1* mutant reproductive growth under severely low B condition.
(A) Aerial portions of Col-0, *tmn1-1*, *tmn1-2* and *tmn1-3* grown hydroponically for 75 d under 0.1, 0.3, 100 and 500 μM B conditions under long-day conditions. Scale bars =20 mm. (B) Magnified pictures of a floral organ and siliques in Col-0, *tmn1-1*, *tmn1-2* and *tmn1-3* grown under 0.3 μM B condition. Scale bars =10 mm. (C) Roots of 75-d-old plants in Col-0, *tmn1-1*, *tmn1-2* and *tmn1-3* under 0.1, 0.3, 100 and 500 μM B conditions. Scale bars =20 mm. .

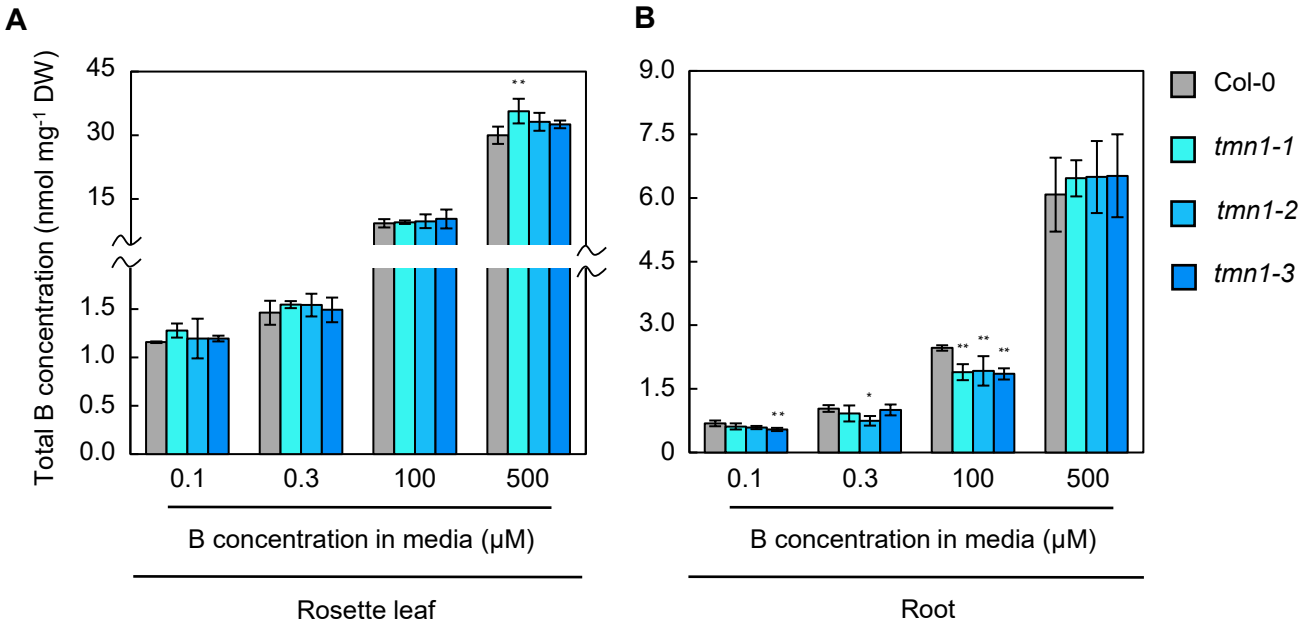

Figure 8. No substantial reduction in total B concentration in the *tmn1* mutants under sufficient B conditions.
Total B concentrations in rosette leaves (A) and roots (B) of Col-0, *tmn1-1*, *tmn1-2* and *tmn1-3*. The plants were grown hydroponically under 0.1, 0.3, 100 and 500 μM B conditions for 45 d under short-day conditions. Values represent means ± SD from four independent samples for rosette leaves and roots. Significant differences between Col-0 and the *tmn1* mutants under each B condition are indicated as **P*<0.05, ***P*<0.01 (Dunnett's multiple comparison test).

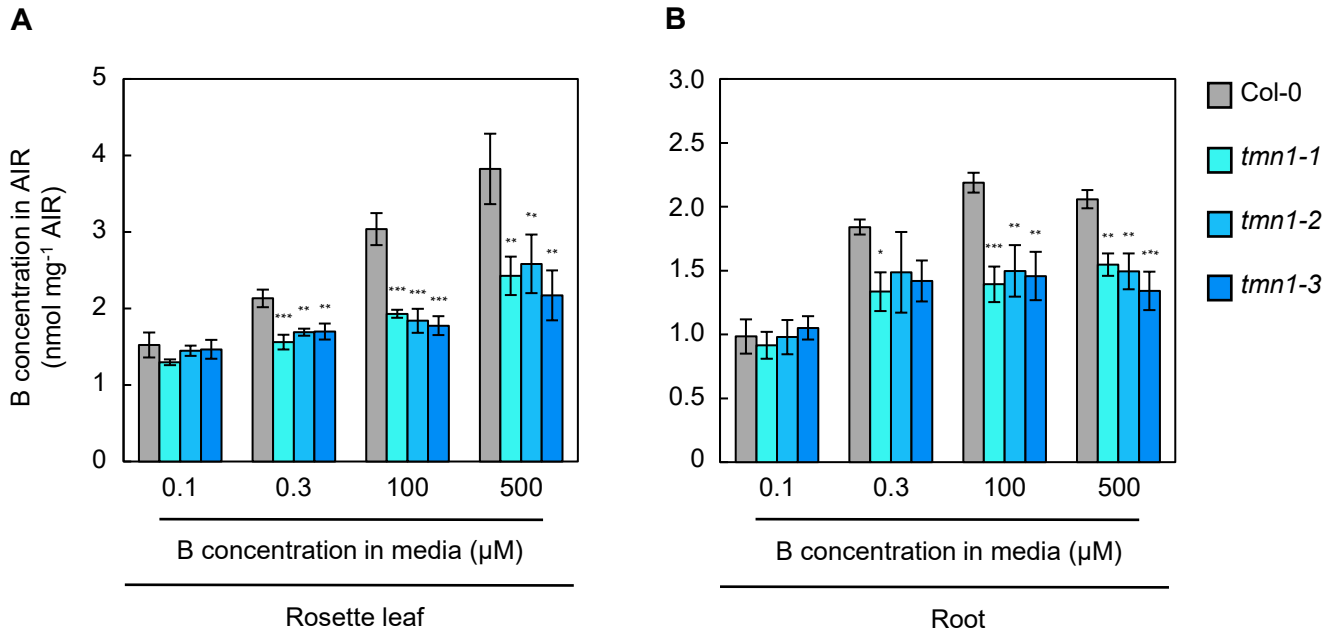

Figure 9. Reduced cell wall B concentrations in *tmn1* mutants under mildly low to high B conditions.
B concentrations in rosette leaf (A) and root (B) cell walls of Col-0, *tmn1-1*, *tmn1-2*, and *tmn1-3* plants grown hydroponically under 0.1 μM, 0.3 μM, 100 μM, and 500 μM B treatments for 44 d under short days. For each cell wall sample, six individual plants for rosette leaves and four to nine plants for roots were harvested and homogenized. Values are means ± SD from three and four independent cell wall samples for rosette leaves and roots, respectively. Asterisks indicate significant differences between Col-0 and the *tmn1* mutants under each B condition (**P*<0.05, ***P*<0.01, ****P*<0.001; Dunnett's multiple comparison test). AIR, alcohol-insoluble residue.

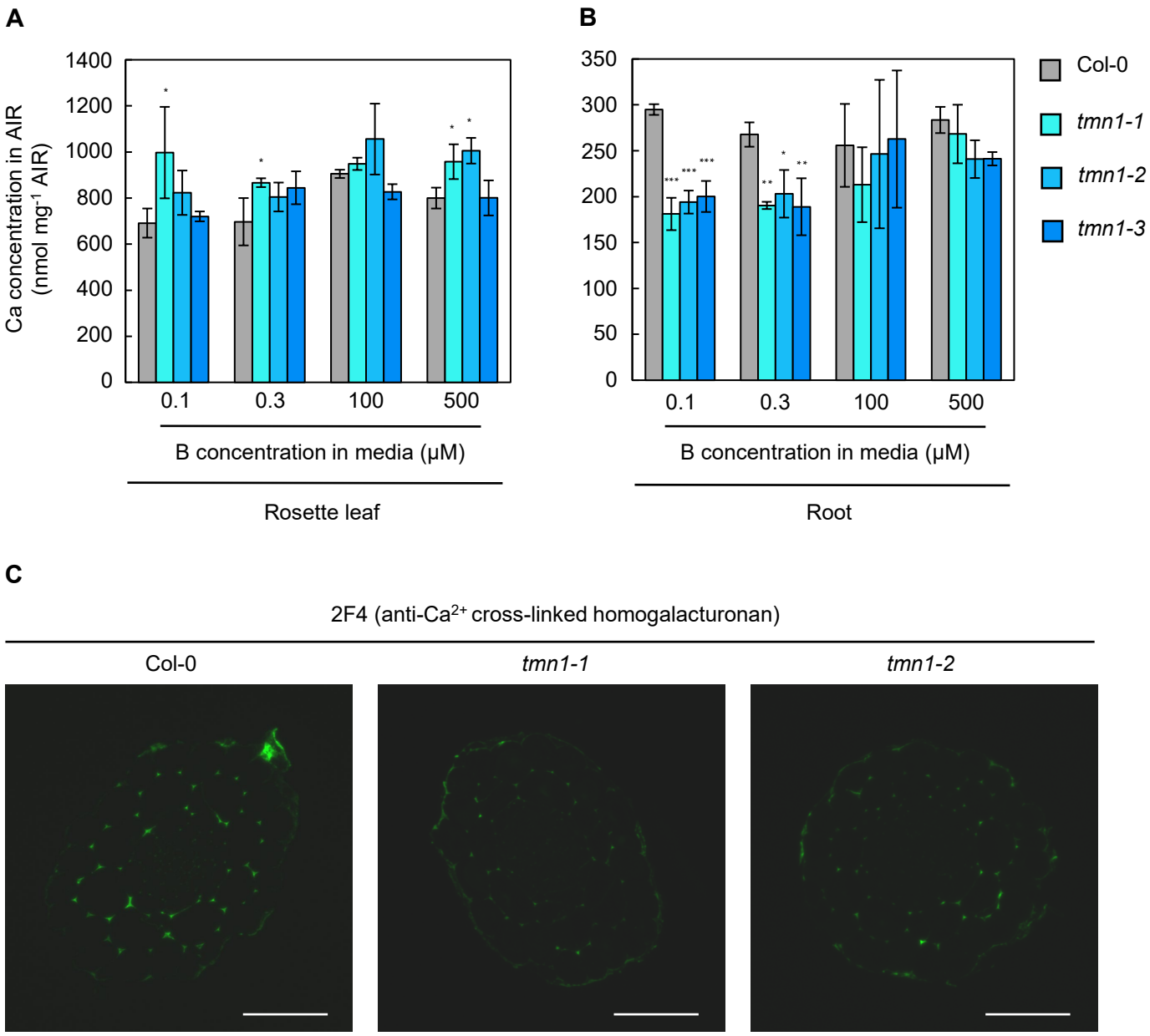

Figure 10. No consistent patterns of changes in cell wall Ca concentrations of the *tmn1* mutants.
Ca concentrations in rosette leaf (A) and root (B) cell walls of Col-0, *tmn1-1*, *tmn1-2* and *tmn1-3*. The plants were grown hydroponically under 0.1, 0.3, 100 and 500 μM B conditions for 44 d under short-day conditions. For each cell wall sample, six individual plants for rosette leaves and four-nine plants for roots were harvested and homogenized. Values represent means ± SD from three and four independent cell wall samples for rosette leaves and roots, respectively. Significant differences between Col-0 and the *tmn1* mutants under each B condition are indicated as **P*<0.05, ***P*<0.01, ****P*<0.001 (Dunnett's multiple comparison test). AIR, alcohol-insoluble residue. (C) Immunohistochemistry of root cross-sections in elongation zone of PRs with an anti-Ca^{2+} cross-linked homogalacturonan antibody (2F4). Plants were grown on solid media under 0.1 μM B condition for 5 d. Scale bars =50 μm.

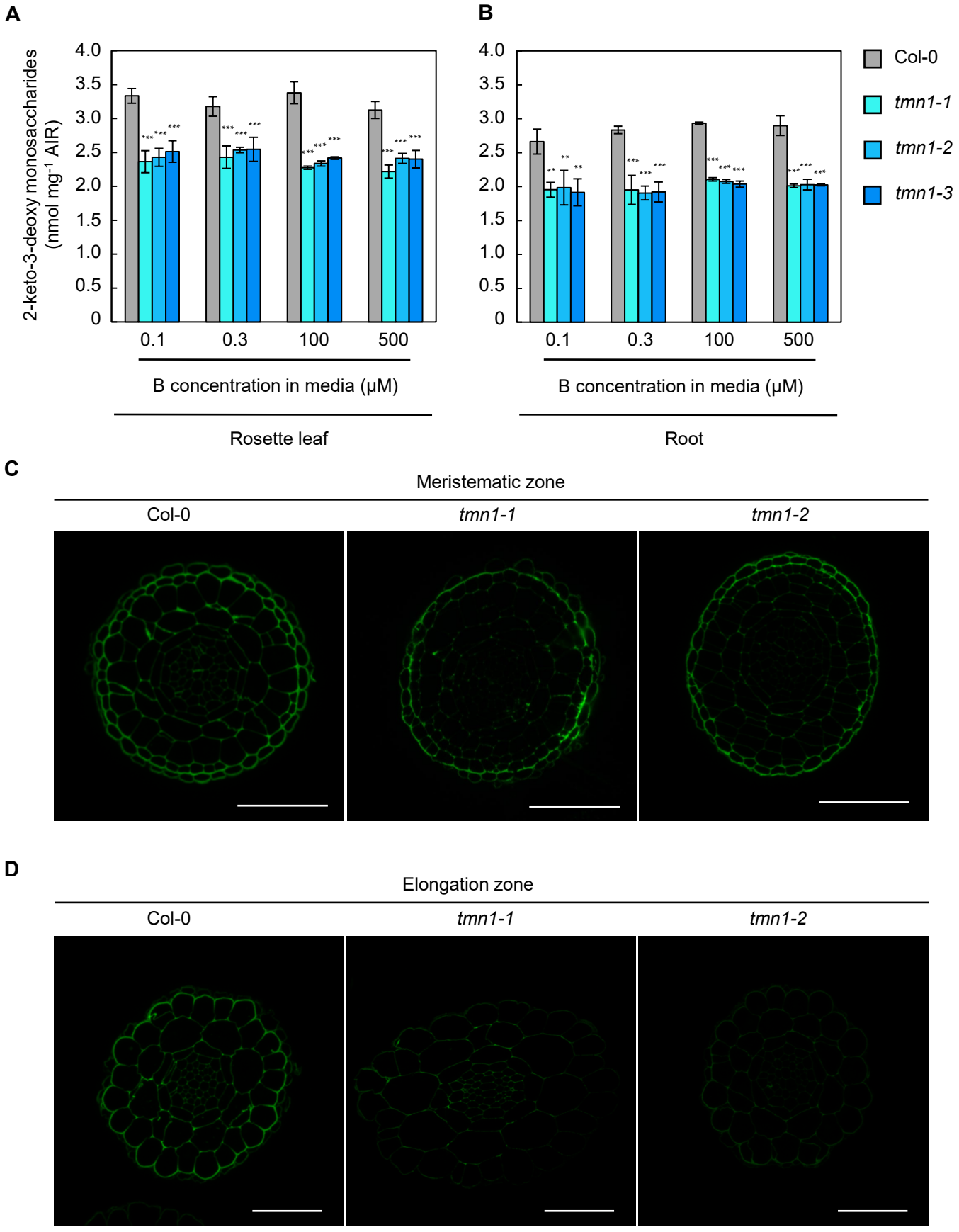

Figure 11. Reduced cell wall RG-II content in the *tmn1* mutants.
Concentration of 2-keto-3-deoxy sugars in rosette leaf (A) and root (B) cell walls of Col-0, *tmn1-1*, *tmn1-2*, and *tmn1-3* plants grown hydroponically under 0.1 μM, 0.3 μM, 100 μM, and 500 μM B treatments for 44 d under short days. For one individual cell wall sample, rosette leaves of three to six plants and roots of six to 12 plants were harvested for homogenization. RG-II was solubilized from AIRs by EPG treatment and 2-keto-3-deoxy sugar concentrations were measured using a modified thiobarbituric acid method. Values are means ± SD from four independent cell wall samples. Asterisks indicate significant differences between Col-0 and the *tmn1* mutants under each B condition (***P*<0.01, ****P*<0.001; Dunnett's multiple comparison test). The concentration of 2-keto-3-deoxy sugars was estimated based on the standard curve of 2-keto-3-deoxyoctonate ammonium salt. AIR, alcohol-insoluble residue. Immunohistochemistry of root cross-sections in the meristematic (C) and elongation zones (D) of PRs with an anti-RG-II antibody, 42–6. Plants were grown on solid media containing 100 μM boric acid for 5 d. Scale bars =50 μm.

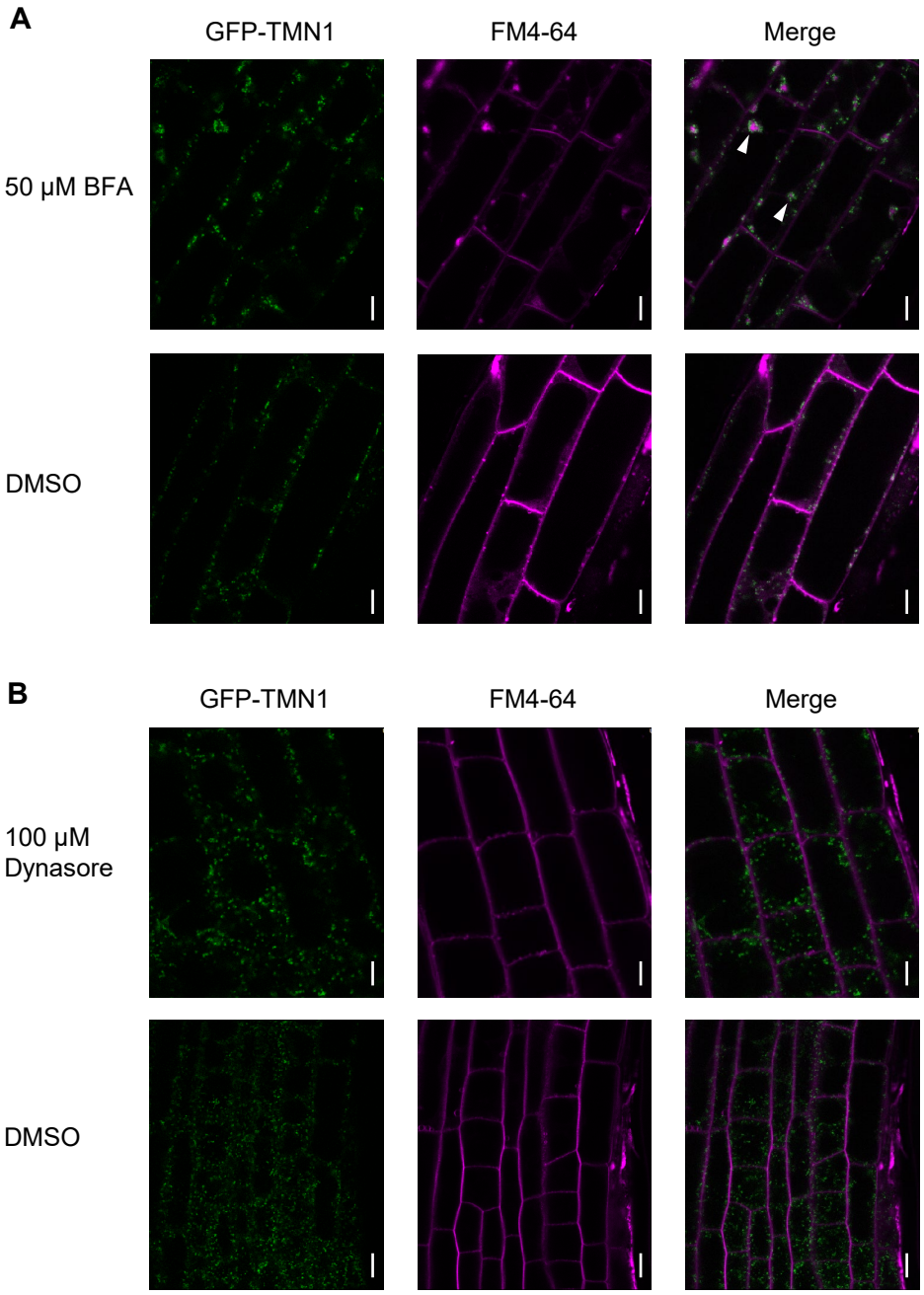

Figure 12. Golgi localization of GFP-AtTMN1 in the presence of BFA and Dynasore.
(A) Sub-cellular localization of GFP-AtTMN1 under BFA treatment. Five-d-old transgenic plants carrying *proAtTMN1:SP(AtTMN1)-GFP-AtTMN1genome* (#1) under 100 μM B were incubated with 2 μM FM4-64 for 5 min and then with 50 μM cycloheximide for 30 min, followed by 50 μM BFA and cycloheximide for 60 min. Arrowheads in dicate ring-like signals of GFP-AtTMN1. (B) Sub-cellular localization of GFP-AtTMN1 under Dynasore treatment. Five-d-old *proAtTMN1:SP(AtTMN1)-GFP-AtTMN1genome* transgenic plants (#1) under 100 μM B conditions were treated with 100 μM Dynasore for 90 min and then with 1 μM FM4-64 for 30 s. Scale bars =10 μm. Similar patterns were observed in the four independent transgenic lines. There are no arrowheads in panel B. If these patterns are observed in B they should also be labelled with arrows. Arrowheads are shown only in panel A. To avoid confusing, we have moved this sentence.